ARTICLE

BIOTECHNOLOGY BIOENGINEERING WILEY

Peptide ligands targeting the vesicular stomatitis virus G (VSV-G) protein for the affinity purification of lentivirus particles

Eduardo Barbieri[1] | Gina N. Mollica[1] | Brandyn D. Moore[1] |
Sobhana A. Sripada[1] | Shriarjun Shastry[1,2] | Ryan E. Kilgore[1] |
Casee M. Loudermilk[1] | Zachary H. Whitacre[1] | Katie M. Kilgour[1] |
Elena Wuestenhagen[3] | Annika Aldinger[3] | Heiner Graalfs[3] | Oliver Rammo[3] |
Michael M. Schulte[3] | Thomas F. Johnson[4] | Michael A. Daniele[5,6] |
Stefano Menegatti[1,2,5,7]

[1]Department of Chemical and Biomolecular Engineering, North Carolina State University, Raleigh, North Carolina, USA

[2]Biomanufacturing Training and Education Center (BTEC), North Carolina State University, Raleigh, North Carolina, USA

[3]Merck KGaA, Darmstadt, Germany

[4]Department of Biochemical Engineering, University College London, London, UK

[5]North Carolina Viral Vector Initiative in Research and Learning (NC-VVIRAL), North Carolina State University, Raleigh, North Carolina, USA

[6]Joint Department of Biomedical Engineering, North Carolina State University and University of North Carolina at Chapel Hill, Raleigh, North Carolina, USA

[7]LigaTrap Technologies LLC, Raleigh, North Carolina, USA

Correspondence
Stefano Menegatti, Department of Chemical and Biomolecular Engineering, North Carolina State University, 911 Partners Way, Raleigh, NC 27606, USA.
Email: smenega@ncsu.edu

Abstract

The recent uptick in the approval of ex vivo cell therapies highlights the relevance of lentivirus (LV) as an enabling viral vector of modern medicine. As labile biologics, however, LVs pose critical challenges to industrial biomanufacturing. In particular, LV purification—currently reliant on filtration and anion-exchange or size-exclusion chromatography—suffers from long process times and low yield of transducing particles, which translate into high waiting time and cost to patients. Seeking to improve LV downstream processing, this study introduces peptides targeting the enveloped protein Vesicular stomatitis virus G (VSV-G) to serve as affinity ligands for the chromatographic purification of LV particles. An ensemble of candidate ligands was initially discovered by implementing a dual-fluorescence screening technology and a targeted in silico approach designed to identify sequences with high selectivity and tunable affinity. The selected peptides were conjugated on Poros resin and their LV binding-and-release performance was optimized by adjusting the flow rate, composition, and pH of the chromatographic buffers. Ligands GKEAAFAA and SRAFVGDADRD were selected for their high product yield (50%–60% of viral genomes; 40%–50% of HT1080 cell-transducing particles) upon elution in PIPES buffer with 0.65 M NaCl at pH 7.4. The peptide-based adsorbents also presented remarkable values of binding capacity (up to $3 \cdot 10^9$ TU per mL of resin, or $5 \cdot 10^{11}$ vp per mL of resin, at the residence time of 1 min) and clearance of host cell proteins (up to a 220-fold reduction of HEK293 HCPs). Additionally, GKEAAFAA demonstrated high resistance to caustic cleaning-in-place (0.5 M NaOH, 30 min) with no observable loss in product yield and quality.

1 | INTRODUCTION

The recent swath of FDA approvals of ex vivo cell therapies—ABECMA™ and CARVYKTI™ for multiple myeloma (U.S. Food and Drug Administration, 2021, 2022a), BREYANZI™ for B-cell lymphoma (U.S. Food and Drug Administration, 2022b), SKYSONA™ for cerebral adrenoleukodystrophy (U.S. Food and Drug Administration, 2022c), and ZYNTEGLO™ for β-thalassemia (U.S. Food and Drug Administration, 2022d)—has turned the spotlight on lentiviruses (LVs) as a replication-defective viral vector for gene and cell therapy (Crespo-Barreda, 2016; Vigna & Naldini, 2000). LVs contain a single-strand RNA, packed inside a capsid and enveloped by a coat with 80–100 nm diameter (Han, 2012; Priori et al., 2018; Robbins et al., 2003; Yaniz-Galende & Hajjar, 2014). The envelope displays many copies of vesicular stomatitis virus glycoproteins G (VSV-G), which preside on virus stability and cellular tropism (Burns et al., 1993). The VSV-G protein interacts with the low-density lipoprotein receptor (LDL-R) on the membrane of the target cell and mediates virus infection by membrane fusion (Finkelshtein et al., 2013).

Despite their clinical relevance, LVs do not yet benefit from an established biomanufacturing platform. In particular, the downstream segment of bioprocessing represents a critical bottleneck in the industry, causing high waiting times and cost to patients (up to $2.8 million per treatment) (Pagliarulo, 2022). LVs are traditionally produced by transfection of packing plasmids and a transfer plasmid with the gene of interest in adherent or suspension HEK293 cells. Following virus production, mammalian cells and debris are removed from the cell culture fluid (CCF) by centrifugation and/or microfiltration. After clarification, different purification processes are employed, including tangential flow filtration, size-exclusion chromatography (SEC; Leung et al., 2020; Perry & Rayat, 2021), ultra-centrifugation (Cribbs et al., 2013), PEG precipitation (Kutner et al., 2009), and anion-exchange chromatography (AEX) on membranes (Cribbs et al., 2013; Kutner et al., 2009; Leung et al., 2020; Moreira, Faria, et al., 2021), nanofibers (Ruscic et al., 2019), monoliths (Bandeira et al., 2012), or resins (Moreira, Faria, et al., 2021). These unit operations, however, suffer from long process time and low scalability as well as limited recovery of LV particles and host cell proteins (HCPs) removal.

The recent consolidation of an industrial layout for manufacturing of adeno-associated viruses (AAVs)—inspired by the downstream process platform established for monoclonal antibodies (Gao et al., 2020; Kozorog et al., 2023; Matos et al., 2021; Zhang et al., 2015)—highlights the role of affinity chromatography as the keystone in the purification of viral vectors for cell and gene

therapies (Fortuna et al., 2019; Moleirinho et al., 2020). For AAVs, a number of affinity adsorbents are available: POROS™ CaptureSelect™ AAVX and AVB Sepharose HP are commercially available as pan-selective resins, while CaptureSelect™ AAV8 and AAV9, and AVIPure® AAV2, AAV8, and AAV9 are available for serotype-specific applications (Adams et al., 2020; van Lieshout et al., 2023). These resins offer excellent product yield (50%–60%) and purity (Florea et al., 2023; Nass et al., 2018), but require harsh elution conditions (pH ~2.5) that can cause product degradation and aggregation, resulting in a loss of transduction activity. Conversely, the commercial offer for LV is less developed. Heparin has been applied as a pseudo-affinity ligand with reported values of recovery ~20%–50% and 95% removal of HCPs (de las Mercedes Segura et al., 2008; Segura et al., 2007). However, heparin is extracted from animal tissues, which poses concerns of contamination (Van der Meer et al., 2017), thus discouraging its use in Good Manufacturing Processes (GMPs) processes (Food & Administration, 2013); moreover, heparin-based adsorbents are not compatible with typical cleaning in place (CIP) procedures used in biomanufacturing, as they rapidly lose selectivity and over 50% of their binding capacity after the first caustic cleaning (Birger Anspach et al., 1995). Other affinity strategies described in the literature rely on the expression of affinity tags on the LV envelope. Cheeks et al. produced histidine-tagged LV particles enabling purification via immobilized metal affinity chromatography (Cheeks et al., 2009); monoliths functionalized with sodium iminodiacetate and nickel showed 69% elution efficiency, but modest binding capacity (6.7×10^8 transducing units per mL of adsorbent, TU/mL, corresponding to ~10^{11} viral particles [vp] per mL of adsorbent; Cheeks et al., 2009); furthermore, the use of imidazole in the elution buffer causes virus inactivation (Ye et al., 2004). In another approach, Mekkaoui et al. applied streptavidin-functionalized magnetics beads for purification of LV particles displaying a cTag8 (Mekkaoui et al., 2018), obtaining yields >60%, and 3-log and 2-log reduction of host cell DNA and HCPs, respectively; however, yield reduced to 20% when the ligands were transferred onto monoliths. More recently, the team led by Peixoto utilized a library of single-domain camelid antibodies (V_HH) to identify ligands targeting the VSV-G protein (Moreira et al., 2023; ThermoFisher, 2023). The ligands, now commercialized in a chromatographic resin format (CaptureSelect™ Lenti VSVG Affinity Matrix), provide a binding capacity of ~10^{11} viral particles per mL of resin (vp/mL) and afford good product purity, while mandating energic elution conditions (0.8 M arginine) and withstanding mildly caustic CIP (10–25 mM aqueous NaOH) (Moreira et al., 2023).

Inspired by that work, our team sought to develop VSV-G-targeting peptides that combine high binding selectivity and capacity

with milder elution conditions and stronger chemical stability and lifetime. A first ensemble of peptides was discovered by screening a focused library of 8-mer peptides against the ectodomain of VSV-G. Ligand selection was implemented using a device established by our team to promote the identification of sequences with bespoke biorecognition activity (Barozzi et al., 2020; Chu et al., 2021; Chu et al., 2022; Day et al., 2019; Kilgore et al., 2023; Lavoie et al., 2021; Prodromou et al., 2021; Sripada, 2023). Following the successful LV purification using the peptides identified experimentally, we pursued the in silico discovery of VSV-G-targeting peptides designed as linear and cyclic mimetics of the LDL-R. These combined efforts delivered the first known set of peptide ligands for LV purification, whose purification performance (i.e., binding capacity, product yield, and clearance of contaminants) and reusability are evaluated and optimized in this study.

2 | RESULTS

2.1 | Selection of chromatographic buffers for library screening

LV particles are highly sensitive to the physicochemical properties of the aqueous environment and their transduction activity can be irreversibly damaged by small variations of pH (Higashikawa & Chang, 2001), salt concentration (Ghosh et al., 2022), temperature (Higashikawa & Chang, 2001), and osmotic pressure (Coroadinha et al., 2006). In the context of bioprocessing, this limits the latitude of chromatographic buffers suitable for LV purification (Kumru et al., 2018). Particularly stringent is the limitation on elution pH, which—being confined to the range of 6–8 (Ye et al., 2003)—cannot be leveraged as in the affinity purification of antibodies (Mazzer et al., 2015) and AAVs (Florea et al., 2023). Accordingly, following published work (Deb et al., 2017; Ghosh et al., 2022; Perry & Rayat, 2021), we explored different formulations of binding and elution buffers that are compatible with LV, initially focusing on citrate-, phosphate-, and histidine-based solutions with different ionic strength and pH. Preliminary stability studies conducted by incubating 10^8 TU/mL, corresponding to ~10^{10} vp per mL, of the various buffers for 30 min (Supporting Information: Figure S1) indicated (i) no significant loss of infectious titer in citrate and phosphate buffers with 75 mM NaCl at pH 6.0 and 7.0; (ii) significant reduction in infectivity (>40%) in 20 mM histidine buffer with 75 mM NaCl at pH 6.0. To formulate the elution buffer, we opted for increasing ionic strength, using sodium chloride and magnesium chloride, in lieu of decreasing pH. Magnesium chloride in sodium citrate buffer did not affect LV activity at pH 6.0 at concentrations ranging from 100 to 500 mM (Supporting Information: Figure S1). Based on these results, we elected 20 mM phosphate buffer with 75 mM NaCl at pH 6.5 and 20 mM citrate buffer with 500 mM $MgCl_2$ at pH 6.0, respectively, as equilibration and elution buffers for library screening.

2.2 | Identification of LV-targeting candidate peptide ligands

The LV vectors utilized in ex vivo applications—including all FDA-approved therapeutics ABECMA, CARVYKTI, BREYANZI, SKYSONA, and ZYNTEGLO (U.S. Food and Drug Administration, 2021, 2022a, 2022b, 2022c, 2022d)—have been designed by pseudotyping (Escors & Breckpot, 2010). This approach consists of replacing the wildtype envelope glycoprotein gp120, which underlies the HIV virus' tropism for human CD4$^+$ T cells, with heterologous glycoproteins. Most LV pseudotyping to date employs the VSV-G (Akkina et al., 1996; Naldini et al., 1996; Reiser, 1996), which endows the vector particles with high stability and the ability to transduce a wide variety of cell types by targeting a ubiquitous cell membrane phospholipidy (Burns et al., 1993; Coil & Miller, 2004; Dautzenberg et al., 2021a). Other proteins utilized for LV pseudotyping—namely the feline endogenous virus (RD114) envelope glycoprotein, the Measles virus hemagglutinin and fusion glycoproteins, the Gibbon ape leukemia virus envelope protein, the Rabies virus glycoprotein, and the Moloney murine leukemia virus 4070A-envelope protein (amphotropic) (Dautzenberg et al., 2021a; Hanawa et al., 2002)–have not provided comparable efficacy. Accordingly, VSV-G-pseudotyped LVs are expected to be utilized in the design of ex vivo cell therapies in the foreseeable future (U.S. Food and Drug Administration, 2021, 2022a, 2022b, 2022c, 2022d).

Under this premise, we elected two model targets for ligand selection, namely the single VSV-G protein and mature VSV-G-pseudotyped LV particles. The VSV-G protein comprises 3 domains, namely the ectodomain (^{E}VSV-G), which is displayed on the viral surface, the transmembrane domain, which anchors the protein in lipid layer of the viral envelope, and the cytoplastic domain (Cleverley & Lenard, 1998; Donas, 1988). While, in principle, only the ^{E}VSV-G can be targeted by surface-immobilized ligands, no information is available on the role of either the transmembrane domain or the intercalation of the full-length VSV-G (^{FL}VSV-G) in the lipid layer on the tertiary structure of the ectodomain. Accordingly, to avoid biasing the ligand selection towards a model target that is not representative of the product, we adopted both ^{E}VSV-G and ^{FL}VSV-G for library screening (Ci et al., 2018; Ferlin et al., 2014).

The selection of candidate peptide ligands was initially performed by screening a solid-phase peptide library using a device for ligand development introduced and demonstrated by our team in prior work (Chu et al., 2022; Kilgore et al., 2023; Prodromou et al., 2023; Sripada et al., 2022). Our technology relies on orthogonal fluorescence labeling to ensure the selection of ligands that possess strong and selective binding, but can also release the target when exposed to mild elution conditions. To this end, we designed a microfluidic bead-imaging-and-sorting device installed in a fluorescence microscope, which we routinely utilize to implement a protocol for peptide ligand discovery (Figure 1): (i) the solid-phase peptide library, produced as a one-bead-one peptide library on hydrophilic and translucent porous particles, is incubated with the target labeled
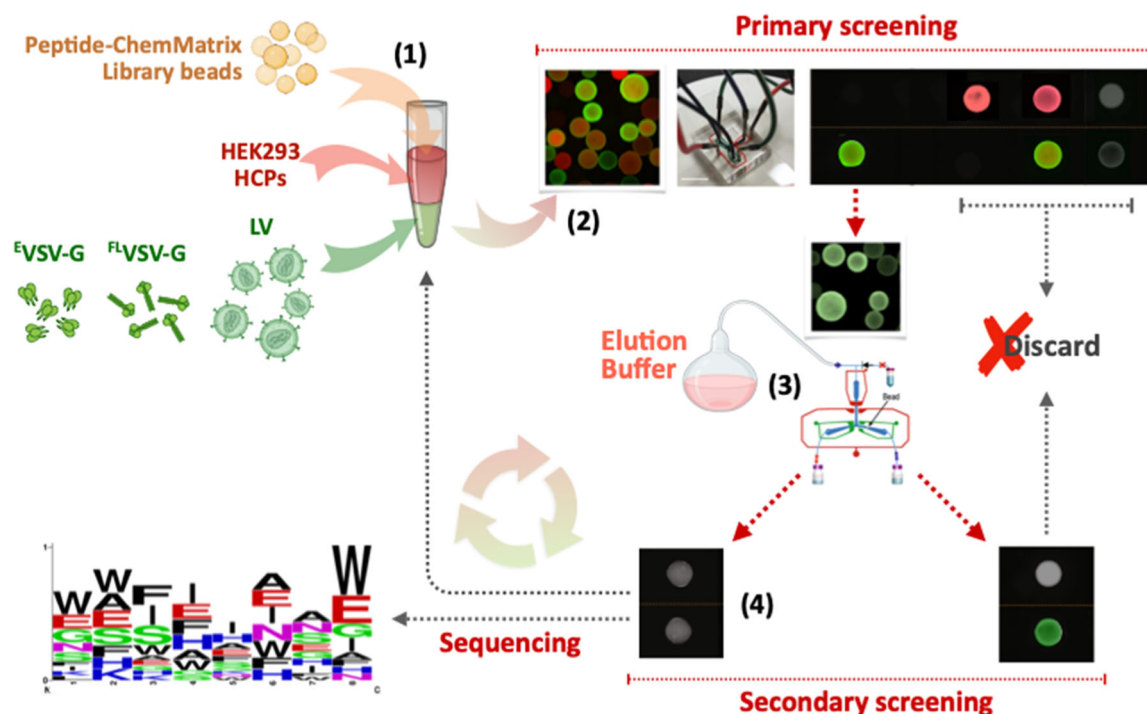
FIGURE 1 Identification of candidate LV-binding peptide sequences. (a) A screening mix was initially formulated containing red-fluorescently labeled HEK293 HCPs at the titer of 0.3 mg/mL and either green-fluorescently labeled LVs at the titer of ~10^9 TU/mL or green-fluorescently labeled VSV-G proteins (^{E}VSV-G and ^{FL}VSV-G) at the titer of 0.2 mg/mL; (b) aliquots of 100 μL of 8-mer peptide-ChemMatrix library beads equilibrated in 20 mM PBS with 75 mM NaCl at pH 6.5 were incubated with 250 μL of screening mix for 30 min at room temperature; (c) the beads were washed and individually fed to a microfluid bead sorting device connected to a fluorescent microscope, wherein (d) each bead that displays high green fluorescence emission and green-to-red signal ratio was retained, while all other beads were discarded; (e) every retained bead was washed with 20 mM citrate buffer with 0.5 M $MgCl_2$ pH 6.0 for 5 min and imaged again; (f) beads that did not show loss of green fluorescence emission were discarded, whereas (g) beads that lost fluorescence signal were collected in 96-well plates; (h) after washing with 0.1 M glycine pH 2.5, water and 30% acetonitrile in water (v/v), the collected beads were individually analyzed by Edman degradation on PPSQ-33A protein sequencer (Shimadzu) to identify the peptide sequences carried thereupon; finally, (i) the sequences identified by screening the library against full LV particles, ^{E}VSV-G ectodomain, and ^{FL}VSV-G FL were grouped in homology plots via Weblogo.

with a green fluorescence dye and a multiplicity of impurities—herein, the whole HEK293 cell proteome—collectively labeled with a red fluorescent dye (*note*: to mimic industrial LV harvests, the screening mix was formulated with an HCP titer of ~0.3 mg/mL and either an LV titer of ~10^9 TU/mL or a VSV-G titer (^{E}VSV-G or ^{FL}VSV-G) of 0.2 mg/mL; herein, Alexafluor 488 and Alexafluor 594 were adopted as the green and red dye, respectively, owing to their low propensity to alter the structure and behavior of the labeled protein); (Hayashi-Takanaka et al., 2014) (ii) following incubation, the library beads are thoroughly washed and individually fed to the microfluidic device, where they are imaged and the image metrics are analyzed in real time; (iii) a bead that displays high green-only fluorescence, denoting selective and strong target affinity, is withheld in the imaging chamber, while all other beads are ejected; (iv) the bead is then exposed to a flow of selected elution buffer—herein, 20 mM citrate buffer with 0.5 M $MgCl_2$ pH 6.0—and imaged again; (v) the beads that display a strong loss of green fluorescence, denoting the ability to release the product under elution conditions defined by the operator, are selected, while all other beads are discarded. The steps (i)–(v) are

automated by a custom Matlab code, which enables conducting the library screening at a rate of 350 beads per hour. Finally, (vi) the sequences carried by the selected beads are identified via Edman Degradation. The list of the peptides identified against ^{E}VSV-G, ^{FL}VSV-G, and full LV particles is reported in Supporting Information: Table S1, while the sequence homology plots are reported in Figure 1i. The identified sequences are ostensibly amphiphilic, each containing at least one aromatic (Phe or Trp) and multiple aliphatic (Ala, Ile) amino acids. Rather notable is the presence of one glutamic acid residue (Glu) in 72% of the identified sequences and two residues in 30% of the sequences. The presence of Glu was unexpected due to the negative charge of the LV surface (Rodrigues et al., 2008), rooted in the phospholipid bilayer forming the envelope, which has made anion exchange chromatography the primary method of separation (McNally et al., 2014; Perry & Rayat, 2021). At the same time, the hydrophilic and anionic character of the candidate ligands reduces the risk of binding HCPs, which requires peptides rich in cationic and hydrophobic amino acids (Lavoie et al., 2019, 2020, 2021; Sripada et al., 2022).

2.3 | Evaluation of candidate peptide ligands in dynamic conditions

Most of the chromatographic resins in the market feature a pore diameter ranging between 20 and 100 nm. While suitable for the purification of protein-based biologics, these adsorbents are not ideal for large viral vectors like LVs and baculovirus, whose diameter can reach 100 nm. Accordingly, the bioseparation community envisions that chromatographic substrates with large pore diameters, such as membranes and monoliths, will become mainstream in the downstream processing of viral vectors (Adams et al., 2020; Alele & Ulbricht, 2016; Carvalho et al., 2019; Kawka et al., 2021; Minh & Kamen, 2021; Moleirinho et al., 2021; Segura et al., 2011). While we fully anticipate the future development of custom-made membranes functionalized with selected peptides, in this work, we resolved to evaluate the selected peptides using established chromatographic adsorbents to avoid uncertainties related to peptide surface density and display. Notably, Poros™ 50 OH resin features pores with diameter of up to 1000 nm and is therefore well suited for the purification of LV particles.

We first modified the Poros™ 50 OH beads by converting its hydroxyl groups to primary amino groups, reaching a functional density of 172 μmol per g of resin (Supporting Information: Figure S2), which were utilized for the conjugation of the sequences identified via library screening (Supporting Information: Table S1). The resulting peptide-Poros resins were evaluated for LV binding and elution in dynamic conditions by loading a clarified HEK293 CCF

(LV titer ~10^{10} vp/mL, corresponding to ~10^8 TU/mL, and HCP titer ~0.3 mg/mL; *note*: some variability in the titer of total and transducing LV particles was observed across different production batches) at the residence time (RT) of 3.5 min recommended for Poros™ resins and using the binding and elution buffers selected in Section 2.1 (namely, 20 mM phosphate with 75 mM NaCl at pH 6.5 and 20 mM citrate buffer with 0.5 M MgCl$_2$ at pH 6.0, respectively).

The values of LV yield and purity listed in Supporting Information: Table S2 point at SIEINSSE, GEFENINW, EWKAAFIW, SKSAAEHE, GKEAAFAA, SNEIEIAN, and FEKISNAE as promising ligand candidates: specifically, these sequences afforded a 10-to-70-fold reduction of HEK293 HCPs and up to 70% reduction of cell DNA; and values of LV genome yield ranging between 30% and 50%. Given the vulnerability of LV particles to changes in buffer composition, conductivity, and pH—that often cause a substantial loss of infectivity—we resolved to quantify the transduction activity of the purified LVs on HT1080 human fibrosarcoma cells as an additional metric to guide the choice of candidate ligands. The values of LV recovery afforded by the selected sequences, collated in Table 1 along with other purification parameters, demonstrate that FEKISNAE and GKEAAFAA perform comparably to control affinity adsorbents Poros™ 50 HE Heparin and CaptureSelect™ Lenti VSVG affinity resins, providing yields of transducing LV particles between 38% and 41%. These values, however, are viewed as rather low when framed in the context of achieving affordable manufacturing of LVs.

Seeking to improve the values of LV yield, we first investigated the effect of residence time of the loading step. The amount of

TABLE 1 Values of LV yield measured via p24 ELISA (viral particles), qPCR (viral genomes), and transduction assay in HT1080 cells (transducing units), together with clearance of HEK293 HCPs obtained by purifying LVs from a HEK293 CCCF (LV titer ~10^{10} vp/mL, corresponding to ~10^8 TU/mL; HCP titer ~0.3 mg/mL) using peptide-Poros resins and control Poros™ 50 HE Heparin and CaptureSelect™ Lenti VSVG affinity resins.

| | RT: 3.5 min | | | | RT: 1 min | | | |
| | Yield | | | | Yield | | | |
Ligand	Viral particles	Viral genomes	Transducing units	HCP LRV	Viral particles	Viral genomes	Transducing units	HCP LRV
EWKAAFIW	12%	40%	22%	0.84	5%	51%	15%	1.33
FEKISNAE	16%	44%	22%	1.62	9%	69%	38%	1.82
GEFENINW	14%	51%	4%	1.73	6%	13%	12%	2.71
GKEAAFAA	15%	34%	17%	1.44	10%	63%	41%	1.87
SIEINSSE	4%	42%	6%	1.69	2%	84%	8%	2.49
SKSAAEHE	8%	32%	25%	1.24	5%	59%	29%	1.75
SNEIEIAN	23%	28%	4%	1.84	12%	65%	12%	2.25
Heparin	19%	20%	18%	1.44	13%	52%	39%	1.79
CaptureSelect™ Lenti VSVG[a]	6%	38%	43%	1.94	[b]			

Note: The purification processes comprised a loading step in 20 mM phosphate buffer with 75 mM NaCl at pH 6.5, at the RT of either 1 or 3.5 min; elution was conducted in 20 mM citrate buffer with 0.5 M MgCl$_2$ at pH 6.0.

[a]Tested according to product instructions: RT of 2 min; equilibration and washing buffer: 50 mM HEPES buffer with 150 mM NaCl at pH 7.5; elution buffer: 50 mM HEPES buffer with 150 mM NaCl and 0.8 M arginine at pH 7.5; stripping solution: 50 mM sodium phosphate at pH 12.0.

[b]Values not measured.

clarified HEK293 CCF loaded on the columns—namely, 30 mL, calculated based on a reference value of load of ~$3 \cdot 10^{11}$ vp per mL of resin (ThermoFisher, 2023) and the LV titer of ~10^{10} vp/mL in the feedstock—when loaded at the flow rate of ~0.3 mL/min (RT of 3.5 min), results in a total loading time of 1.75 h. Combined with the duration of the harvest and clarification steps, chromatographic washing and elution steps, and incubation of purified LVs with HT1080 cells, this brings the total process time to about 3 h. Comparing this time to the half-life of VSV-G pseudotyped LVs at room temperature—estimated at 35 h (Dautzenberg et al., 2021)—suggests that the values of recovery of transducing LVs may be negatively impacted by the long processing time. To obviate this inconvenience, we conducted additional testing of select peptides by reducing the residence time of all chromatographic steps from 3.5 to 1 min, which shortened the processing time from 3 h to about 50 min. Specifically, we focused on the sequences GEFENINW and SNEIEIAN, selected based on the recovery of LV particles and genomes, as well as FEKISNAE, EWKAAFIW, SKSAAEHE, GKEAA-FAA, selected based on the recovery of transducing LV particles. The results collated in Table 1 show that reducing the load residence time proved beneficial to the performance of all resins: in particular, the yield of FEKISNAE, GEFENINW, and GKEAAFAA increased 1.7-to-3-fold, while their HCP clearance grew from an LRV of 1.4–1.6 to 1.8–2.7; notably, the product yield and purity afforded by Poros™ 50 HE Heparin also doubled, indicating that the need of a shorter loading time is not tied to a particular chemical composition of the ligands. It is also worth noticing that the performance of the peptide-based adsorbents is comparable to that of the control affinity resins, in terms of recovered viral particles and genomes as well as purity. At the same time, with the values of yield well below 50%, further process optimization is necessary to improve the economics of LV production.

2.4 | Optimizing LV purification by adjusting the composition of the chromatographic buffers

The growth of LV yield and purity obtained simply by reducing the residence time of the loading step suggests that further adjustment of the chromatographic process is in order. Accordingly, we undertook the optimization of the composition, concentration, and pH of the chromatographic buffers to improve the performance of FEKISNAE-, GEFENINW-, and GKEAAFAA-Poros resins. To that end, we initially explored the addition of arginine to the wash buffer and MgCl$_2$ to the elution buffer, and subsequently evaluated buffers with different basal compositions and conductivity, while maintaining a constant RT of 1 min for the loading step.

As shown in Table 2, the addition of 50 mM arginine to the wash buffer (20 mM phosphate buffer with 75 mM NaCl at pH 6.5) slightly increased the HCP LRV obtained with FEKISNAE-Poros resin from 1.82 to 2.01 (corresponding to a 102-fold reduction and a residual HCP titer of less than 3 μg/mL, or <10^{-11} μg/vp), suggesting a potential strategy to improve HCP clearance. However, increasing

the MgCl$_2$ concentration from 0.5 to 1 M in the base elution buffer (20 mM citrate buffer at pH 6.0) reduced LV recovery and was therefore abandoned.

We therefore resolved to explore additional buffer systems with different basal compositions. Based on studies conducted by Ghosh et al. (2022) and Perry and Rayat (2021), we first adopted Tris to formulate new equilibration, wash, and elution buffers. Notably, the new wash buffer (50 mM Tris buffer with 130 mM NaCl at pH 8.0) increased the HCP LRV by FEKISNAE-Poros resin to 2.39 (corresponding to a 246-fold reduction and a residual HCP titer of 1.2 μg/mL, or <$5 \cdot 10^{-12}$ μg/vp) and that of GKEAAFAA-Poros resin to 2.05 (112-fold reduction; 2.6 μg/mL or <10^{-11} μg/vp). Additionally, the new elution buffer (50 mM Tris and 1 M NaCl at pH 8.0) increased the yield of transducing LV particles afforded by FEKISNAE- and GKEAAFAA-Poros to 35% and 38%, respectively. Under the same conditions, GEFENINW-Poros resin provided excellent purity, but unsatisfactory yields; this poor performance, combined with the presence in this peptide of asparagine (N) and tryptophan (W) residues that are prone to degradation – chiefly, deamidation to aspartic acid (Linhult et al., 2004) and oxidation (Bellmaine et al., 2020)—led us to abandon this candidate ligand.

We then proceeded to evaluate HEPES and PIPES buffers. The stabilization effect that these buffers have demonstrated on LV particles (Deb et al., 2017; Kumru et al., 2018; Moreira, Cavaco, et al., 2021) and the ability of heparan sulfate and Chondroitin Sulfate to bind LV particles (whether or not VSV-G pseudotyped) (Sun &, 2014, 2014; Volland et al., 2021) suggest that sulfonic acid groups interact favorably with LV particles (Deb et al., 2017). Accordingly, we evaluated a new set of wash and elution buffers—50 mM HEPES/PIPES buffer at pH 7.4 added with 100 mM and 0.65 M NaCl, respectively—starting with GKEAAFAA as the top-performing ligand. The results summarized in Figure 2 show an appreciable improvement in both the yield of transducing LV particles and HCP clearance, which reached respectively a value of 51% and an LRV of 2.26 (i.e., 182-fold reduction; residual titer ~1.6 μg/mL, corresponding to <$5 \cdot 10^{-12}$ μg/vp or <$3 \cdot 10^{-8}$ μg/TU) using PIPES-based buffers. Accordingly, four more candidate sequences—namely FEKISNAE, and the candidate ligands SKSAAEHE, EWKAAFIW, and EHFEHWSE, selected from Supporting Information: Table S2 based on their sequence similarity with GKEAAFAA and FEKISNAE—were reevaluated using the PIPES-based buffers. The resulting chromatograms are in Supporting Information: Figure S3, while the corresponding values of LV yield and purity are collated in Table 3. Collectively, these results strongly support the adoption of piperazineethanesulfonate-based buffers, and, more broadly, showcase the impact of chromatographic processing on the transduction activity of the purified LV particles: while no reduction was in fact observed upon incubation of LV particles in either HEPES and PIPES buffers, chromatographic processing caused an appreciable loss of infectivity (i.e., purified LV particles exhibited almost half of the transduction activity of their pre-chromatography counterparts when tested on HT1080 cells at the same viral genome-to-cell ratio). This suggests the need to adopt different chromatographic substrates, such as membranes and monoliths—which will be

TABLE 2 Values of LV recovery measured via p24 ELISA (total particles), qPCR (total viral genomes), and transduction assay in HT1080 cells (transducing particles), together with clearance of HEK293 HCPs and DNA obtained by purifying LVs from a HEK293 CCCF (LV titer ~10^{10} vp/mL, corresponding to ~10^8 TU/mL; HCP titer ~0.3 mg/mL) using FEKISNAE-, GEFENINW-, and GKEAAFAA-Poros resins.

| Ligand | Buffers | | | Yield | HCP LRV |
	Binding	Wash	Elution		
FEKISNAE		20 mM phosphate	20 mM citrate	8%	1.81
	20 mM phosphate	75 mM NaCl, pH 6.5	0.5 M MgCl$_2$, pH 6.0		
	75 mM NaCl, pH 6.5	20 mM phosphate		13%	2.01
		100 mM NaCl	20 mM citrate		
		50 mM arginine, pH 6.5	0.5 M MgCl$_2$, pH 6.0		
	50 mM Tris	50 mM Tris	50 mM Tris	38%	2.39
	130 mM NaCl, pH 8.0	130 mM NaCl, pH 8.0	1 M NaCl, pH 8.0		
GEFENINW	20 mM phosphate	20 mM phosphate	20 mM citrate	1%	2.39
			1 M MgCl$_2$, pH 6.0		
	75 mM NaCl, pH 6.5	75 mM NaCl, pH 6.5	20 mM citrate	1%	2.37
			0.5 M MgCl$_2$, pH 6.0		
	50 mM Tris	50 mM Tris	50 mM Tris	<1%	1.92
	130 mM NaCl, pH 8.0	130 mM NaCl, pH 8.0	1 M NaCl, pH 8.0		
GKEAAFAA	20 mM phosphate	20 mM phosphate		28%	1.83
		100 mM NaCl	20 mM citrate		
	75 mM NaCl, pH 6.5	50 mM arginine, pH 6.5	0.5 M MgCl$_2$, pH 6.0		
	50 mM Tris	50 mM Tris	50 mM Tris	35%	2.05
	130 mM NaCl, pH 8.0	130 mM NaCl, pH 8.0	1 M NaCl, pH 8.0		

Note: All purification processes comprised a loading step conducted at the RT of 1 min. The values of yield were measured via transduction activity on HT1080 cells.
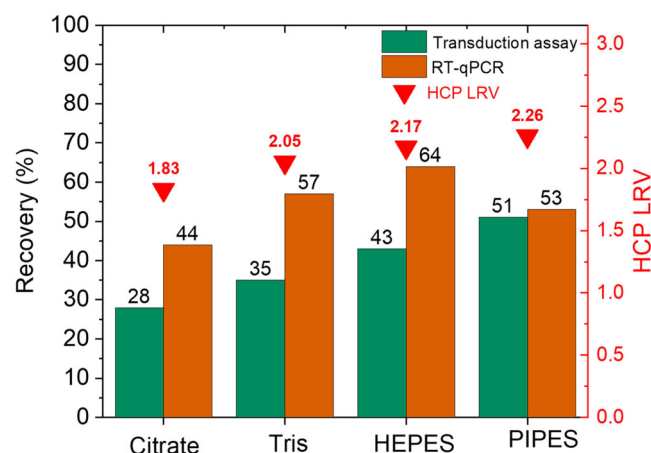

FIGURE 2 Values of LV recovery measured via p24 ELISA (total particles), qPCR (total viral genomes), and transduction assay in HT1080 cells (transducing particles), and clearance of HEK293 HCPs (orange histogram) obtained by purifying LVs from a HEK293 CCF (LV titer ~10^{10} vp/mL, corresponding to ~10^8 TU/mL; HCP titer ~0.3 mg/mL) using GKEAAFAA-Poros resins; the loading step was operated at the RT of 1 min. The values of yield were measured via p24 ELISA (green histogram), qPCR (blue histogram), and transduction activity on HT1080 cells (teal histogram).

explored in future work—whose wider porosity reduces the mechanical stress on LV particles and their residence time in the process.

2.5 | In silico discovery and experimental evaluation of VSV-G-binding peptides

The results presented in the previous sections demonstrate that the peptide sequences identified by screening the peptide library against VSV-G consistently outperformed the sequences selected against full LV particles. This points to the rational design of sequences that target ligand-able sites on VSV-G as a promising route to the discovery of peptide ligands for LV purification. In this context, particularly helpful are the published crystal structure of the complex formed by VSV-G and the cysteine-rich domains of the LDL-R (CR2 and CR3), a cell surface receptor that plays a key role in LV cell entry (Nikolic et al., 2018). Notably, the team that resolved and analyzed the structure of this complex identified two cationic residues on VSV-G, His8, and Lys47, that target anionic residues Asp69 and Asp 73 on CR2 and Asp108 and Asp112 on CR3, and provide a major contribution to the LDL-R binding energy. Additionally, the LDL-R

TABLE 3 LV purification using an optimized chromatographic protocol. Values of LV recovery measured via p24 ELISA (total particles) and qPCR (total viral genomes), logarithmic removal value of HEK293 host cell proteins (HCP LRV), and residual double-strand DNA obtained via chromatographic purification of LV particles from a HEK293 CCF (LV titer ~10^{10} vp/mL, corresponding to ~10^8 TU/mL; HCP titer ~0.3 mg/mL) using peptide-Poros resins.

	Yield			
Ligand	Viral particles	Viral genomes	HCP LRV	Residual dsDNA
SKSAAEHE	52%	54%	1.81	23%
EWKAAFIW	17%	33%	2.08	46%
GKEAAFAA	48%	74%	2.07	33%
EHFEHWSE	13%	27%	2.32	11%
FEKISNAE	63%	55%	2.39	45%

Note: The equilibration and washing steps were conducted using 50 mM PIPES buffer with 100 mM NaCl at pH 7.4 (RT: 1 min); elution was conducted using 50 mM PIPES buffer with 0.65 M NaCl at pH 7.4 (RT: 1 min).

CR2 and CR3 domains feature a compact tertiary structure, rigidly held by 3 disulfide bonds, which resembles that of scaffolds (i.e., knottins, avimers, and bicyclic peptides) (Frejd & Kim, 2017; Vazquez-Lombardi et al., 2015) utilized to discover small protein affinity ligands. Finally, the analysis of pairwise interactions between the active residues on LDL-R CR2 and CR3, reported in Supporting Information: Figure S4 and Table S3, indicates that the VSV-G binding site consists of a continuous segment of residues. Relevant to this work, these data suggest that (i) small peptide mimetics of LDL-R CR2 and CR3 can be designed in silico to target the same CR-binding site of VSV-G; and (ii) the top-performing ligands identified via library screening—SKSAAEHE, GKEAAFAA, and FEKISNAE—all of which contain at least one glutamic acid residue, may indeed target the LDL-R CR-binding site of VSV-G.

Accordingly, we designed an in silico ensemble of candidate ligands, whose sequence and structure mimic the LDL-R CR2 and CR3 domains: specifically, the four disulfide-cyclic sequences C-cyclo[GSRQFVADSDRD]C-GSG, C-cyclo[GSRSFVGDSDRD]C-GSG, C-cyclo[GSRAFVADADRD]C-GSG, C-cyclo[GSRAFVGDAD]C-GSG, and the five linear sequences SRQFVCGDSDRD-GSG, SRSFVCDSDRD-GSG, SRAFVGDADRD-GSG, AFVGDADRD-GSG, and SFVRIGLSD-GSG. The sequence homology and the small values of root-mean-square deviation (RMSD) of the atomic positions of the designed peptides versus their cognate CR2 and CR3 domains provide confidence in the LDL-R-mimetic behavior of the proposed sequences. The eight designed peptides, along with SKSAAEHE, GKEAAFAA, FEKISNAE, and the latter's variants FEKISAAE and FEKISTAE, were docked in silico against the crystal structures of VSV-G (PDB IDs: 5OY9 and 5OYL) in different aqueous environments that represent the various buffers utilized during the purification process, namely ionic strength and pH of 150 mM and 7.4 to represent the binding buffer, and 0.7 M and pH 7.4 or 1 M and

pH 6.0 representing two alternative elution buffers (namely, 50 mM PIPES buffer with 0.65 M NaCl at pH 7.4; 20 mM citrate with 0.5 M MgCl2, pH 6.0). Peptide docking was focused on the putative binding sites identified on the solvent-accessible surface of the protein as "ligandable", namely whose physicochemical and topological characteristics make it apt to bind a biomolecular ligand with true affinity (Surade & Blundell, 2012). The other key constraint imposed during docking is for the -GSG tripeptide appended on the C-terminal end not to interact with the target VSV-G: this forces the -GSG tripeptide to orient outward from the binding pose, thus mimicking the orientational constraint imposed to the peptides by their conjugation on the surface of the chromatographic resin. In prior studies, this constraint has been delivered with superior accuracy in estimating the target binding energy (Bacon et al., 2020; Barozzi et al., 2020; Chu et al., 2022; Day et al., 2019; Kilgore et al., 2023; Reese et al., 2020). The resultant VSV-G:peptide complexes, selected based on their cluster size and initial scoring using X-Score (Wang et al., 2003), were subjected to 250-ns MD simulations in explicit-solvent conditions that represent the binding and elution buffers to obtain reliable values of binding free energy (ΔG_b). Selected complexes are shown in Figure 3 and the corresponding values of the dissociation constant ($K_{D,\text{in silico}}$) are listed in Table 4.

The results of molecular docking support the design criteria of the mimetic sequences: (i) all peptides, with the sole exception of SKSAAEHE, formed complexes whose binding pairwise interactions recapitulate those of the VSV-G:LDL-R complexes; (ii) the binding strength of the VSV-G:peptide complex in the binding environment is moderately lower (5.9–8.7 kcal/mol; $K_D \sim 5 \cdot 10^{-7}$ to $5 \cdot 10^{-6}$ M) than that of their VSV-G:LDL-R CR2 and CR3 precursors (9.3–9.7 kcal/mol; $K_D \sim 5 \cdot 10^{-8}$ to 10^{-7} M); and (iii) all peptides except SRTFVCDSDRD exhibited comparable affinity for a second binding site (described by the green surface in Figure 3). The ability of peptide ligands to target multiple binding sites on the target surface with true affinity suggests the formation of a multi-site interaction network between the virus and the peptide-functionalized surface. This mechanism has been observed in prior studies on the de novo discovery of peptide ligands for AAV purification (Chu et al., 2023) to be conducive to high capacity and selective binding as well as efficient product recovery under mild elution conditions. The LV coat displays approximately 216 VSV-G proteins (Croyle et al., 2004), suggesting that VSV-G are placed at 12.5–31.3 Å from each other (assuming the LV radius to be 40 – 50 nm); additionally, based on the peptide density on the resin (~30 µmol per gram) and the resin's specific surface (~30 m^2/g), the peptides are displayed at ~18 Å from each other. This suggests the formation of 8–10 VSV-G:peptide interactions per bound LV particle. The cooperation of multiple affinity interactions results in a strong avidity-like binding that promotes efficient and selective LV capture, as demonstrated by the values of binding capacity and product purity presented below (Section 3.6).

Furthermore, as shown in Table 4, the dissociation constant (K_D) of the VSV-G:peptide complexes undergo a 540-to-750-fold increase as the ionic strength of the environment increases from 150 mM to
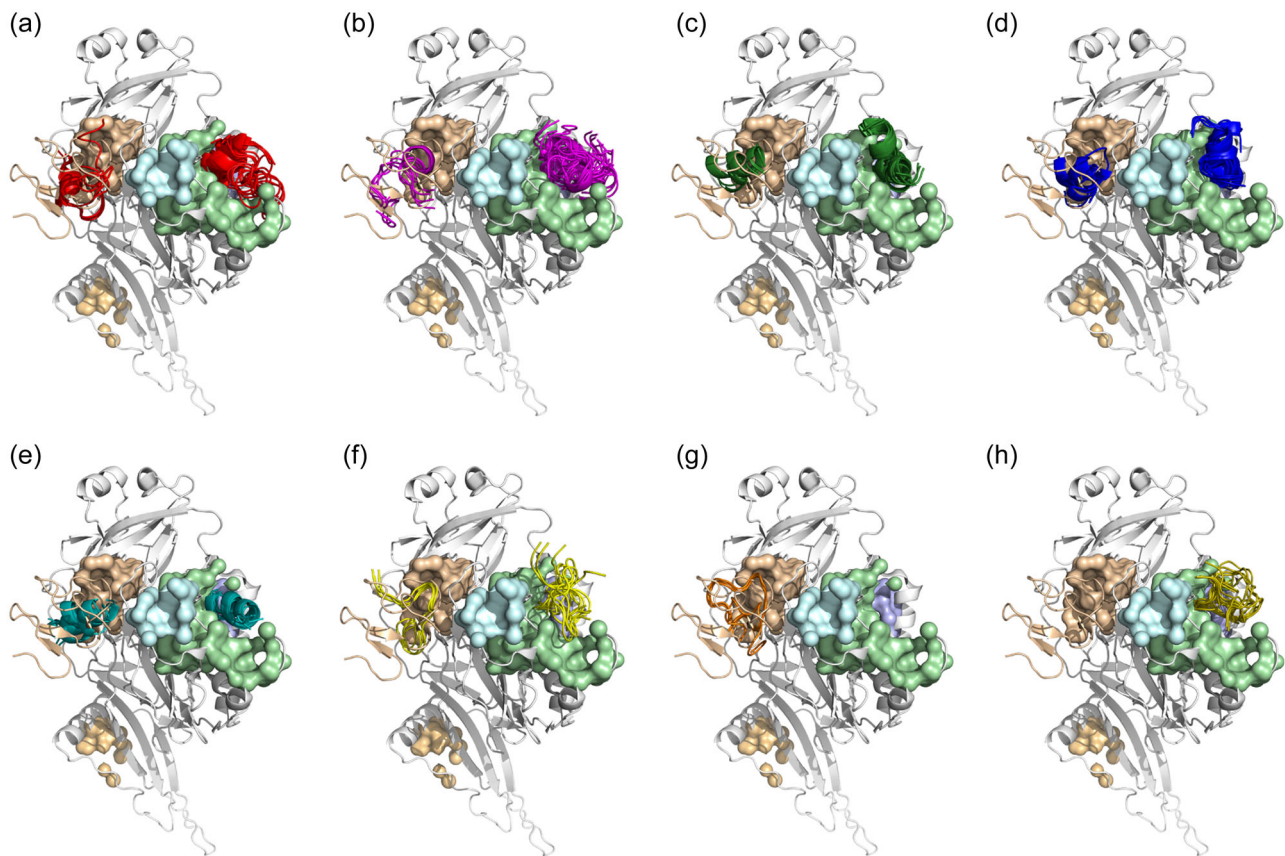
FIGURE 3 Complexes formed by VSV-G with peptides (a) C-cyclo[GSRQFVADSDRD]C-GSG (red), (b) C-cyclo[GSRSFVGDSDRD]C-GSG (magenta), (c) FEKISAAE-GSG (green), (d) FEKISNAE-GSG (blue), (e) GKEAAFAA-GSG (teal), (f) SRQFVCDSDRD-GSG (yellow), (g) SRTFVCDSDRD-GSG (orange), and (h) SVFRIGLSD-GSG (mustard). The VSV-G and LDL-R are presented as gray and wheat cartoons, respectively; the interacting amino acids on VSV-G and LDL-R are in dark blue and red, respectively. The putative binding sites identified via druggability study of the solvent-accessible surface of VSV-G are presented as wheat, light blue, light green, and light brown surfaces.

1.3 M (representing the 50 mM PIPES elution buffer containing 0.65 M MgCl$_2$) and a 1550-to-1900-fold increase as the pH decreases from 7.4 to 6.0 (representing the 20 mM citrate elution buffer). This suggests that the adsorbed viruses can be effectively released under conditions that safeguard their transduction activity, as confirmed by the values of product yield (vide infra and Section 3.4). The analysis of the molecular simulation trajectories indicates that the VSV-G:peptide dissociation is strongly influenced by the loss of (i) Coulombic interactions between the anionic residues in the peptide ligands and their cationic counterparts on the VSV-G, chiefly Lys47, Arg342, and Arg354, which contribute ~34%–41% of the binding energy at pH 7.4.

The second major contributor to the free energy of binding, the network of hydrogen bonds and polar interactions—chiefly those formed with Gln10, Ser179, Asn180, Ser183, Thr350-352, and Glu353, which contribute 31%–39% of the binding energy—is also obliterated by the addition of MgCl$_2$—a known chaotrope—which destabilizes the electrostatic and hydrogen bonding interactions (Salvi et al., 2005; Zhou & Pang, 2018). The increase of ionic strength and the decrease of pH also causes a contraction of the VSV-G solvent-accessible pockets: albeit small, this rearrangement

significantly reduces the structural complementarity of the putative pockets to the peptide ligands and promotes their dislodging from the coat proteins. The energy of both VSV-G:LDL-R CR2 and CR3 complexes is also reduced when the simulation environment is switched to elution conditions. However, their residual strength at the reference elution conditions (ΔG_b ~7.2–8.2 kcal/mol) is higher than what was observed among the VSV-G:peptide complexes, suggesting that product elution from protein ligands is more challenging; this could explain why stronger denaturing conditions are required for LV elution from antibody-based ligands (e.g., 0.8 M arginine is recommended for elution from CaptureSelect™ Lenti VSVG affinity resin).

Based on the predicted values of VSV-G affinity at pH 7.4 and loss of binding upon application of elution conditions, peptides C-cyclo[GSRAFVGDAD]C, SRQFVCGDSDRD, SRAFVGDADRD, and SFVRIGLSD were conjugated on Poros resins and evaluated by purifying LVs from a clarified HEK293 cell culture harvest using the optimized PIPES-based buffer system. The results summarized in Table 5 confirm the criteria adopted in the in silico peptide design: the cyclic peptide afforded the highest value of HCP clearance registered in this study (i.e., residual HCP titer ~0.34 μg/mL, or

TABLE 4 Values of dissociation constant ($K_{D, in silico}$) of the complexes formed by LDL-R-mimetic peptides designed in silico and the peptides identified via library screening with VSV-G obtained via molecular docking and dynamics simulations in explicit solvent conditions that mimic the binding (ionic strength of 150 mM and pH of 7.4) and elution (A: 0.7 M and pH 7.4; B: 1 M and pH 6.0) buffers.

Ligand	CR2/3 versus peptide RMSD (Å)	Site 1 (LDL-R binding site)			Site 2		
		Binding (M)	Elution A (M)	Elution B (M)	Binding (M)	Elution A (M)	Elution B (M)
C-cyclo[GSRQFVADSDRD] C-GSG	2.37	$1.05 \cdot 10^{-6}$	$6.57 \cdot 10^{-5}$	$4.64 \cdot 10^{-5}$	$5.05 \cdot 10^{-7}$	$6.50 \cdot 10^{-5}$	$9.66 \cdot 10^{-5}$
C-cyclo[GSRSFVGDSDRD] C-GSG	2.56	$1.00 \cdot 10^{-6}$	$6.68 \cdot 10^{-5}$	$4.77 \cdot 10^{-5}$	$6.05 \cdot 10^{-7}$	$6.82 \cdot 10^{-5}$	$1.07 \cdot 10^{-4}$
C-cyclo[GSRAFVADADRD] C-GSG	2.47	$1.38 \cdot 10^{-4}$	$1.47 \cdot 10^{-4}$	$1.05 \cdot 10^{-4}$	$2.13 \cdot 10^{-4}$	$1.40 \cdot 10^{-4}$	$2.10 \cdot 10^{-4}$
C-cyclo[GSRAFVGDAD] C-GSG	2.42	$1.08 \cdot 10^{-6}$	$1.68 \cdot 10^{-4}$	$1.07 \cdot 10^{-4}$	$5.00 \cdot 10^{-7}$	$1.65 \cdot 10^{-4}$	$2.40 \cdot 10^{-4}$
SRQFVCGDSDRD-GSG	1.95	$1.05 \cdot 10^{-6}$	$1.58 \cdot 10^{-4}$	$1.16 \cdot 10^{-4}$	$5.00 \cdot 10^{-7}$	$1.41 \cdot 10^{-4}$	$2.29 \cdot 10^{-4}$
SRSFVCDSDRD-GSG	1.87	$1.03 \cdot 10^{-5}$	$5.60 \cdot 10^{-5}$	$4.08 \cdot 10^{-5}$	$5.05 \cdot 10^{-5}$	$5.71 \cdot 10^{-5}$	$8.00 \cdot 10^{-5}$
SRAFVGDADRD-GSG	1.81	$1.36 \cdot 10^{-6}$	$8.53 \cdot 10^{-4}$	$7.35 \cdot 10^{-4}$	$6.75 \cdot 10^{-7}$	$8.75 \cdot 10^{-4}$	$1.11 \cdot 10^{-3}$
AFVGDADRD-GSG	1.76	$1.01 \cdot 10^{-4}$	$1.40 \cdot 10^{-4}$	$1.01 \cdot 10^{-4}$	$1.06 \cdot 10^{-4}$	$1.41 \cdot 10^{-4}$	$2.02 \cdot 10^{-4}$
SFVRIGLSD-GSG	1.58	$1.12 \cdot 10^{-6}$	$8.33 \cdot 10^{-4}$	$5.30 \cdot 10^{-4}$	$5.50 \cdot 10^{-7}$	$8.53 \cdot 10^{-4}$	$1.05 \cdot 10^{-3}$
FEKISNAE	[a]	$1.93 \cdot 10^{-6}$	$3.78 \cdot 10^{-4}$	$1.99 \cdot 10^{-4}$	$1.07 \cdot 10^{-6}$	$4.41 \cdot 10^{-4}$	$6.36 \cdot 10^{-4}$
FEKISAAE		$2.74 \cdot 10^{-6}$	$1.84 \cdot 10^{-4}$	$2.31 \cdot 10^{-4}$	$1.38 \cdot 10^{-6}$	$1.91 \cdot 10^{-4}$	$2.73 \cdot 10^{-4}$
FEKISTAE		$1.41 \cdot 10^{-6}$	$5.25 \cdot 10^{-4}$	$1.23 \cdot 10^{-4}$	$9.05 \cdot 10^{-7}$	$5.29 \cdot 10^{-4}$	$9.15 \cdot 10^{-4}$
GKEAAFAA		$3.70 \cdot 10^{-6}$	$1.46 \cdot 10^{-4}$	$3.83 \cdot 10^{-4}$	$1.65 \cdot 10^{-6}$	$1.50 \cdot 10^{-4}$	$2.14 \cdot 10^{-4}$
SKSAAEHE		$1.79 \cdot 10^{-6}$	$5.95 \cdot 10^{-4}$	$1.52 \cdot 10^{-4}$	$9.70 \cdot 10^{-7}$	$4.75 \cdot 10^{-4}$	$7.55 \cdot 10^{-4}$
LDL-R CR2 (5OYL)	–	$1.41 \cdot 10^{-7}$	$6.75 \cdot 10^{-6}$	$9.82 \cdot 10^{-6}$	[b]		
LDL-R CR2 (5OY9)		$6.92 \cdot 10^{-8}$	$5.01 \cdot 10^{-6}$	$3.73 \cdot 10^{-6}$			

[a]Peptides GKEAAFAA, SKSAAEHE, and FEKISNAE and its derivatives FEKISAAE and FEKISTAE were not desired as LDL-R mimetics.

[b]This site is not targeted by the CR2 and CR3 domains of LDL-R.

~10^{-12} μg/vp or <$1 \cdot 10^{-8}$ μg/TU, corresponding to a 871-fold reduction), but returned a rather unsatisfactory amount of product. Conversely, the SRAFVGDADRD and SFVRIGLSD afforded a yield of transducing LV particles comparable to those obtained with FEKISNAE and GKEAAFAA, while still providing >100-fold reduction of HCPs and ~68-fold reduction of DNA, and were therefore selected for further characterization.

These results support the development—in silico or in vitro—of VSV-G-targeting peptides as affinity ligands for the purification of LV from recombinant feedstocks. Owing to their moderate affinity and ability to form multiple interactions leading to strong avidity-driven product capture, VSV-G-targeting peptides can match antibody-based ligands in terms of binding capacity and selectivity, while outperforming them in product yield under non-denaturing conditions. Additionally, the adoption of chemically stable amino acids in constructing the resin-bound library or the in silico ensemble of LDL-R mimetics, and the lack of tertiary structure characteristic of short peptides are conducive to the selection of ligands that are likely more robust than protein binders. The latter aspect is particularly relevant in biopharmaceutical manufacturing, as it impacts the number of uses

that an affinity resin can withstand, which represents a key determinant of the operational costs of a process—and ultimately the price of the drug to patients.

2.6 | Dynamic binding capacity and alkaline stability of peptide-poros resins

Based on the results in Tables 3 and 5, we proceeded to measure the dynamic binding capacity (DBC$_{10\%}$) and stability of adsorbents FEKISNAE-, GKEAAFAA-, SRAFVGDADRD-, and SFVRIGLSD-Poros resins. Unlike the conventional literature, where the values of DBC$_{10\%}$ are measured by loading solutions of pure virus and are therefore not representative of realistic process streams, we opted to conduct our breakthrough experiments by loading a clarified bioreactor harvest containing LV particles at a titer of ~10^8 TU/mL (~10^{10} vp/mL). The measurements were conducted at two values of residence time, namely 2 and 1 min: the former is recommended for CaptureSelect™ Lenti VSVG affinity resin and was adopted in this work for comparability; the latter was adopted to reduce the

TABLE 5 LV purification using LDL-R-mimetic peptides designed in silico. Values of yield (1: LV genomes measured via qPCR; 2: transducing LV particles measured via flow cytometry), logarithmic removal value of HEK293 host cell proteins (HCP LRV), and residual double-strand DNA obtained via chromatographic purification of LV particles in bind-and-elute mode from a HEK293 CCCF (LV titer ~10^{10} vp/mL, corresponding to ~10^8 TU/mL; HCP titer ~0.3 mg/mL) using LDL-R-mimetic peptide-Poros resins.

Ligand	Yield		HCP LRV	Residual dsDNA
	Viral genomes	Transducing viral particles		
C-cyclo[GSRAFVGDAD] C-GSG	16%	12%	2.94	8
SRQFVCGDSDRD-GSG	18%	15%	2.42	25
SRAFVGDADRD-GSG	60%	45%	2.20	32
SFVRIGLSD-GSG	55%	38%	2.02	26

Note: The equilibration and washing steps were conducted using 50 mM PIPES buffer with 100 mM NaCl at pH 7.4 (RT: 1 min); elution was conducted using 50 mM PIPES buffer with 0.65 M NaCl at pH 7.4 (RT: 1 min).

processing time of LV particles and achieve a higher yield of transducing particles. The results reported in Figure 4 and the corresponding values of $DBC_{10\%}$ summarized in Table 6 demonstrate that all peptide-based adsorbents possess high $DBC_{10\%}$, on par with or above the values of commercial affinity resins. Specifically, GKEAAFAA-Poros and SFVRIGLSD-Poros resins featured a remarkable $DBC_{10\%}$ of $1.91 \cdot 10^{10}$ and $3.99 \cdot 10^{10}$ vg/mL (corresponding to ~$5 \cdot 10^{10}$ and $1.5 \cdot 10^{11}$) at the RT of 1 min; FEKISNAE-Poros and SRAFVGDADRD-Poros resins showed slightly lower, yet still appreciable, values of $DBC_{10\%}$ of $5.84 \cdot 10^9$ and $6.89 \cdot 10^9$ vg/mL (RT of 1 min). For reference, the $DBC_{10\%}$ of CaptureSelect™ Lenti VSVG resin is $9.73 \cdot 10^{10}$ vp/mL at the RT of 2 min, while that of Poros™ 50 HE Heparin affinity resin is ~10^8 TU/mL (~10^{10} vp/mL) at the RT of 0.5 min. The ability of peptide-functionalized adsorbents to capture a comparable amount of LV particles while reducing the process time of 50% may stem from the "flexible" biorecognition mechanism of peptide ligands. As suggested by the docking studies, which returned several high-probability binding poses for each sequence (Figure 3), the interactions with VSV-G formed by peptide ligands appear to be less orientation-dependent than those formed by proteins. This may promote the rapid formation of multi-site binding of LV particles by the peptide-functionalized surface—manifested in the form of faster adsorption kinetics—which translates into equal binding capacity at lower residence time or higher capacity at a longer residence time.

We noted that the ratio of LV titer in the effluent (C) did not reach the corresponding value in the load (C_0) at plateau. Food and Administration (2013) also reported a C/C_0 plateau ~0.8 when measuring the LV binding capacity of heparin-functionalized resins. To assess the role of LV loss in the tubing on the plateau value of the LV titer, we loaded HEK293 CCCF on the FPLC system without a column and conducted a transduction assay of the effluent fractions

as soon as they were dispensed on fraction collector. As anticipated, the analysis of the effluents showed a 5%–10% loss in LV transduction activity, which can be ascribed to shear, nonideal temperature, or adsorption on the inner walls of the chromatographic equipment (*note*: our FPLC system is constructed with inert tubes).

Together with binding capacity, another critical parameter in downstream bioprocessing is the resin stability to CIP. The caustic treatments with concentrated aqueous sodium hydroxide (0.1–0.5 M) (Gülich et al., 2000; Horenstein et al., 2003; Łącki & Riske, 2020) established in antibody manufacturing are now being transferred to the production of viral vectors for in vivo and ex vivo gene therapy. Commercial resins POROS CaptureSelect AAVX and AVIPure affinity resins for AAV purification are designed to withstand multiple cycles of reuse with intermediate caustic cleaning (Florea et al., 2023). At present, however, these ligands have not yet reached the chemical stability of latest-generation Protein A for mAb purification, whose decades of engineering have made it capable of withstanding many cycles of cleaning with 0.5 M NaOH (Xia et al., 2014; Zhang et al., 2017). Similarly, the affinity technology for LV purification is still in its infancy, and the newly introduced ligands have not yet accessed the molecular engineering pathway leading to high chemical stability; accordingly, the recommended CIP conditions for Poros™ 50 HE Heparin and CaptureSelect™ Lenti VSVG resins are limited to 25 mM NaOH (Birger Anspach et al., 1995; ThermoFisher, 2023).

The lability of protein-based ligands has often been linked to the deamidation of asparagine/glutamine (N/Q) residues, as observed in native Protein A (Kato et al., 2020), and the loss of tertiary structure caused by the exposure to high pH. Conversely, three of the four selected peptides—namely, GKEAAFAA, SRAFVGDADRD, and SFVRIGLSD—do not contain either N or Q and they only feature a secondary α-helical structure, which can be rapidly recovered upon incubation in neutral pH. On the other hand, FEKISNAE is expected to convert to FEKISDAE when subjected to alkaline cleaning due to the deamidation of N to aspartic acid (D). When exposed to a flow of 50 mM NaOH, in fact, FEKISNAE-Poros resin lost ~50% of its binding capacity and, following a static contact with 0.1 M NaOH for 30 min, did not show any measurable binding of LV particles. Therefore, alkaline-stable variants FEKISAAE and FEKISTAE were designed in silico to possess VSV-G binding and elution activity comparable to those of the cognate sequence (Table 3).

Accordingly, adsorbents GKEAAFAA-, FEKISAAE-, SRAFVG DADRD-, and SFVRIGLSD-Poros resins were subjected to five consecutive cycles of LV purification from the HEK293 CCF with intermediate CIP with 0.5 M NaOH. The lifetime study presented in Figure 5 corroborates the criteria adopted in peptide design. Specifically, GKEAAFAA maintained its binding capacity and selectivity, consistently adsorbing >10^9 TU/mL (>10^{11} vp/mL) and affording an average yield ≥ 40% of transducing LV particles (≥50% by qPCR) and a 130-to-300-fold reduction of HEK293 HCPs (Figure 5a). FEKISAAE demonstrated a purification performance on par with its cognate FEKISNAE, while possessing a significantly higher stability: throughout the five subsequent purification cycles, the adsorbent maintained its capacity (~$5 \cdot 10^8$ TU/mL, ~10^{11} vp/mL) and afforded a
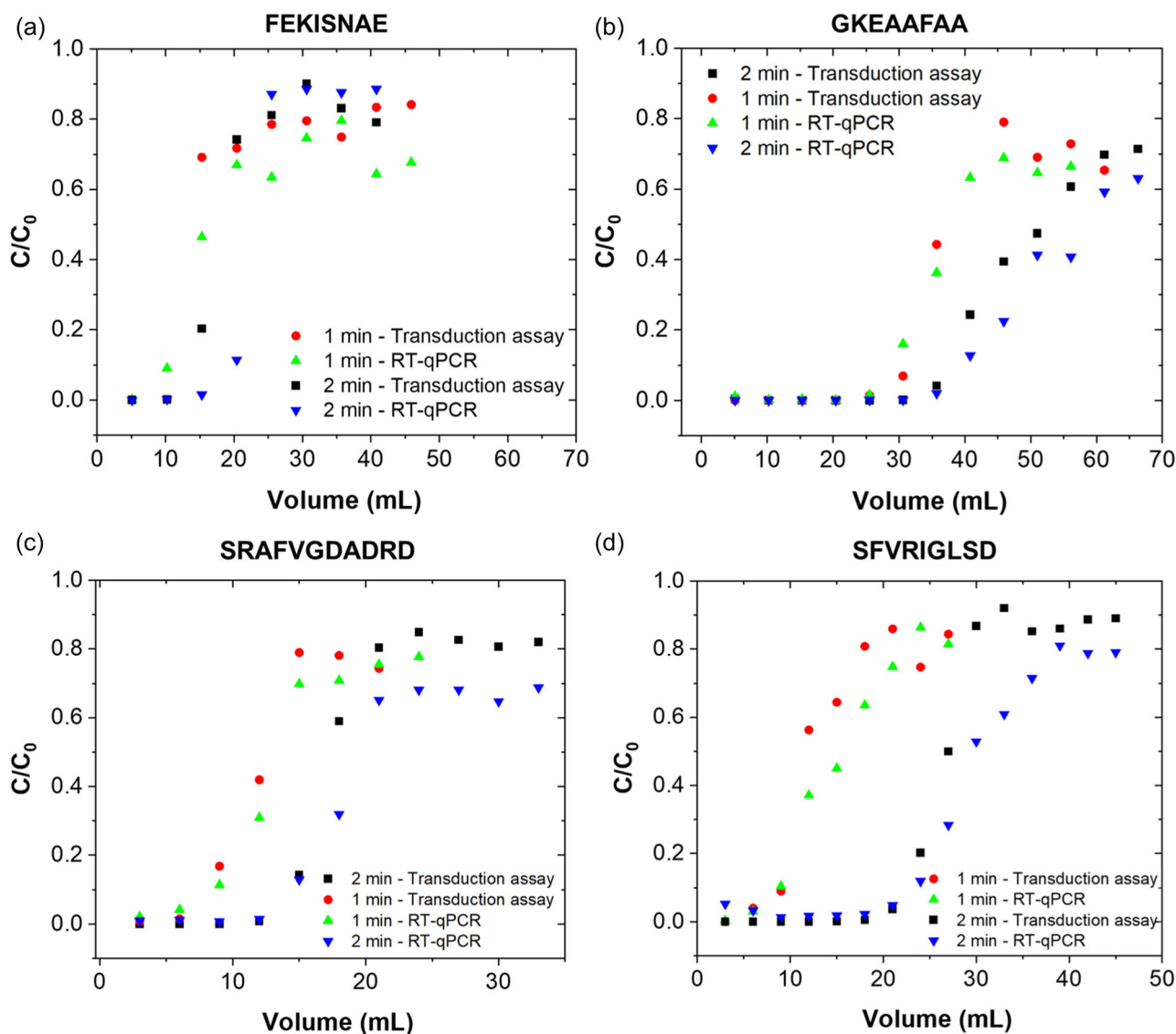
FIGURE 4 Breakthrough curves obtained by loading a HEK293 CCCF (LV titer ~10^{10} vp/mL, corresponding to ~10^8 TU/mL; HCP titer ~0.3 mg/mL) on (a) FEKISNAE-, (b) GKEAAFAA-, (c) SRAFVGDADRD-, and (d) SFVRIGLSD-Poros resins at the residence time of either 1 or 2 min. The LV titer in the effluent was measured via real-time qPCR (vg/mL) and transduction assay (TU/mL).

product yield consistently above 50% together with a >200-fold reduction of HCPs (Figure 5b). Conversely, FEKISTAE-Poros resins displayed a significant reduction of LV bound to column with increasing the number of CIP cycles (*data not shown*); we speculate that the slight acidity of the threonine residue may display a negative charge that lowers the binding capacity of this peptide (Chin et al., 1997). Finally, SRAFVGDADRD and SFVRIGLSD maintained high LV binding and elution yield (~10^9 TU/mL, corresponding to >10^{11} TU/mL, >38%, respectively) as well as impurity clearance across the consecutive cycles.

While longer lifetime studies are needed to consolidate these results, this initial evaluation demonstrates the potential of rationally designed peptides as ligands for the purification of LVs in actual industrial biomanufacturing.

3 | CONCLUSIONS

Lentiviral vectors are rapidly becoming an essential tool for producing lifesaving cell therapies. Their manufacturing technology, however, is in its infancy and can afford limited product volumes, thus limiting the application of these therapies to a small group of patients living in advanced economies. While access to healthcare relies on many factors, introducing biomanufacturing technologies that are productive and robust as well as affordable and scalable is critical toward bringing advanced therapies to fruition to a broader patient population worldwide. In this spirit, our team introduced the first ensemble of peptide ligands for the purification of VSV-G-pseudo typed LVs via affinity chromatography. By integrating criteria of affinity, selectivity, and stability of the peptide sequences

TABLE 6 Values of dynamic LV binding capacity ($DBC_{10\%}$) of peptide-Poros resins loaded with HEK293 CCCF (LV titer ~10^{10} vp/mL, corresponding to ~10^8 TU/mL; HCP titer ~0.3 mg/mL) at the residence time of either 1 or 2 min.

Ligand	RT (min)	$DBC_{10\%}$ (vg/mL)	(TU/mL)
FEKISNAE	1	$7.03 \cdot 10^9$	$1.43 \cdot 10^9$
	2	$5.84 \cdot 10^9$	$1.69 \cdot 10^9$
GKEAAFAA	1	$1.91 \cdot 10^{10}$	$3.04 \cdot 10^9$
	2	$2.69 \cdot 10^{10}$	$4.24 \cdot 10^9$
SRAFVGDADRD	1	$6.89 \cdot 10^9$	$1.31 \cdot 10^9$
	2	$9.63 \cdot 10^9$	$2.30 \cdot 10^9$
SFVRIGLSD	1	$3.99 \cdot 10^{10}$	$1.41 \cdot 10^9$
	2	$8.07 \cdot 10^{10}$	$3.76 \cdot 10^9$
CaptureSelect™ Lenti VSVG	2	$9.73 \cdot 10^9$ vp/mL	
Heparin	0.5	10^8 TU/mL (~10^{10} vp/mL)	

Note: The LV titer in the effluent was measured via real-time qPCR (vg/mL) and transduction assay (TU/mL).

under different user-defined conditions, our discovery strategy delivers ligands with a unique combination of high binding capacity, clearance of impurities, yield of transducing vectors, and lifetime. To demonstrate this approach, we applied these criteria towards the experimental as well as the in silico discovery of VSV-G-targeting peptides. Among the sequences identified via library screening, GKEAAFAA affords a binding capacity of $3 \cdot 10^9$ TU per mL of resin (corresponding to $>10^{11}$ vp/mL), a 60%–70% yield of transducing LV particles, and a reduction of HCPs above 200-fold, while also demonstrating stability to caustic cleaning. Similarly, among the sequences designed in silico, alkaline-stable SRAFVGDADRD and SFVRIGLSD showed a binding capacity above 10^9 TU/mL ($>10^{11}$ vp/mL), 38-45% yield, and >200-fold HCP clearance. As short peptides, these ligands can be affordably produced at scale: recent studies indicate that, when manufactured at the 10 kg scale or above, the cost of 8-mer peptides can be as little as $60 per gram (Bray, 2003). Given that ~25 g of the proposed peptides are required to functionalize a liter of resin, the cost-of-goods of the peptide-functionalized resins would range between $7.5–9K per liter, thus providing a competitive alternative to affinity resins that rely on protein ligands. To further explore the potential of this technology, future work will focus on the evaluation of these peptide ligands for the purification of VSV-G-pseudotyped LVs loaded with different genetic payloads as well as their use on alternative chromatographic substrates such as monoliths and membranes. The latter hold great value to further reducing the residence time during loading, thus minimizing process time and increasing the likelihood of recovering LVs with higher transduction activity.

4 | EXPERIMENTAL

4.1 | Materials

Dimethyl sulfoxide (DMSO), thioanisole, anisole, ethane-1,2-dithiol (EDT), polybrene, citric acid, hydrochloric acid (HCl), magnesium chloride hexahydrate ($MgCl_2 \cdot 6H_2O$), phosphate buffer saline at pH 7.4 (PBS), and Kaiser test kit were obtained from MilliporeSigma. N,N′-Dimethylformamide (DMF), dichloromethane (DCM), carbonyl diimidazole (CDI), viral production cells, LV-MAX production medium, LV-MAX transfection kit, LV-MAX Lentiviral Packaging Mix, Opti-MEM Reduced Serum Medium, Vivid Colors™ pLenti6.3/V5-GW/EmGFP Expression Control Vector, Stbl3™ Chemically Competent *E. coli*, TrypLE™ express enzyme, fetal bovine serum (FBS), PureLink™ HiPure Plasmid Maxiprep Kit, NHS-AlexaFluor 488 (AF488), NHS-AlexaFluor 594 (NHSAF594), Dulbecco's Phosphate Buffered Saline (DPBS), TaqMan™ Fast Virus 1-Step Multiplex Master Mix, TaqMan™ custom made probe and primers, Purelink Viral RNA/DNA Kit, Turbo DNAse, Proteinase K, CaptureSelect™ Lenti VSVG Affinity Matrix, Poros™ 50 HE Heparin affinity resin, Poros™ 50 OH resin, and high glucose DMEM supplemented with GlutaMAX™ and pyruvate were obtained from ThermoFisher Scientific. Fmoc/tBu-protected amino acids, hexafluorophosphate azabenzotriazole tetramethyl uronium (HATU), piperidine, diisopropylethylamine (DIPEA), N-Methyl-2-pyrrolidone (NMP), and trifluoroacetic acid (TFA) were purchased from ChemImpex (Wood Dale, Illinois). T-75 and T-25 cell culture flasks, 96-well culture plates, DNAse/RNAse-free water, and ampicillin were from VWR. Shake flasks and Plasmid⁺ media for bacterial growth were from Thomson. Yeast extract, peptone, and granulated agar were purchased from Genesee Scientific. The HT1080 cell line was received from the American Type Culture Collection (AATC). Tris(hydroxymethyl)aminomethane hydrochloride (Tris-HCl), sodium phosphate monobasic dihydrate, sodium citrate dihydrate, sodium hydroxide (NaOH), and sodium chloride (NaCl) were sourced from Fisher Chemical. Aminomethyl ChemMatrix (particle diameter: 75–150 μm, loading: 0.6 mmol per g resin) resin was from PCAS Biomatrix, Inc. The HIV1 p24 ELISA kits were purchased from Abcam.

4.2 | Expression and purification of ^EVSV-G and ^{FL}VSV-G

The plasmids encoding for Strep-tagged ^{FL}VSV-G and ^EVSV-G were amplified using the pLP/VSVG expression plasmid as template (Invitrogen). HEK293T cells were seeded into 14.5 cm dishes and transfected with the respective plasmids using PEIpro (Polyplus). Harvesting was conducted after 48 h of expression: for ^EVSV-G, expressed as an extracellular product, the cell culture supernatant was collected and sterile filtered through 0.22 μm PES filter (Stericup Quick Release, Millipore); for ^{FL}VSV-G, expressed as an intracellular product, the cells were lysed using Triton X-100 (0.01 M Tris-HCl,
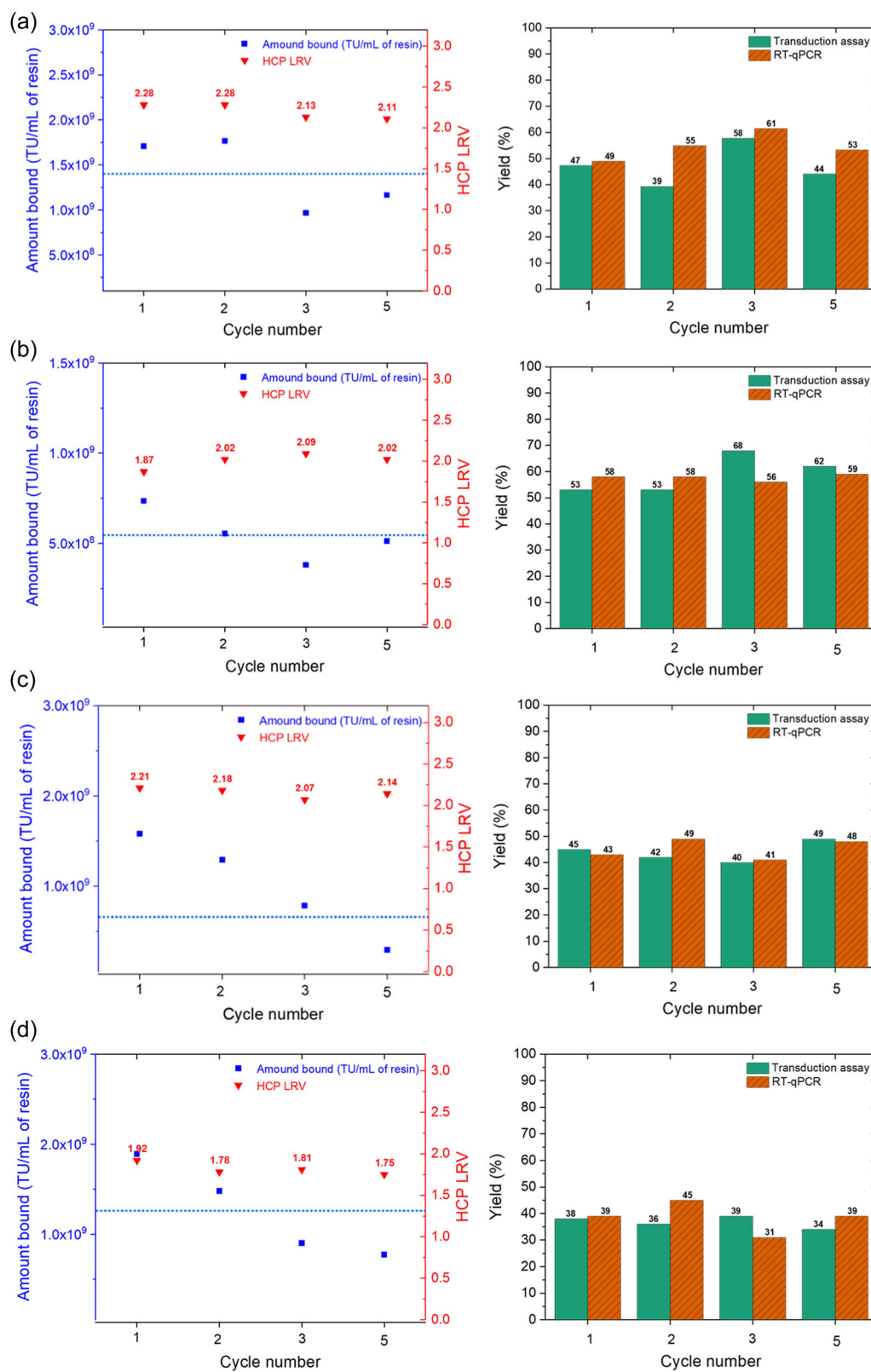
FIGURE 5 Caustic stability study of (a) GKEAAFAA-, (b) FEKISAAE-, (c) SRAFVGDADRD-, and (d) SFVRIGLSD-Poros resins conducted as consecutive cycles of LV purification from the HEK293 CCF with intermediate CIP with 0.5 M NaOH (15 CVs at the RT of 1 min followed by 30 min of static contact time).

2 mM $MgCl_2$, 0.25% Triton X-100, pH 8), centrifugation, and sterile filtration through 0.22 μm PES filter (Millex-GP, Millipore). Both [FL]VSV-G and [E]VSV-G were purified via Strep-tag capture using a 1-mL Strep-Tactin® Superflow® high capacity cartridge (IBA Lifesciences GmbH) using 0.15 M NaCl, 0.1 M Tris-HCl, 0.001 M EDTA as equilibration buffer; 0.1 M Tris-HCl as wash buffer; 0.15 M NaCl, 0.1 M Tris-HCl, 0.001 M EDTA, 0.01 M D-desthiobiotin, 0.25% Triton X-100 as elution buffer for [FL]VSV-G; 0.15 M NaCl, 0.1 M Tris-HCl, 0.001 M EDTA, 0.01 M D-desthiobiotin, 0.006 M n-Octyl-β-D-glucosid as elution buffer for [E]VSV-G; 0.15 M NaCl, 0.1 M Tris-HCl, 0.001 M EDTA, 0.001 M HABA as regeneration buffer. The column was initially equilibrated with 5 CVs equilibration buffer. The centrifuged and sterile-filtered cell culture lysate ([FL]VSV-G) and the cell culture supernatant ([E]VSV-G) were loaded at the flow rate of 78 cm/h. After sample loading, the column was washed with 10 CVs equilibration buffer, and the bound proteins were eluted with 4 CVs of elution buffer at the flow rate of 156 cm/h. Regeneration was performed with 3 CVs of regeneration buffer, followed by a wash with 5 CVs of wash buffer, and re-equilibration with 5 CVs of equilibration buffer. The column was stored in equilibration buffer and used for up to three runs. Elution fractions were aliquoted and stored at −20°C until use.

4.3 | Production of LV particles

The LVs were produced using LV-MAX system (Thermo Fisher Scientific) following the manufacturer's protocol (Gibco, 2021). The plasmid pLenti6.3/V5-GW/EmGFP was transformed in Stbl3 Chemically Competent *E. coli* cells and selected on LB agar plates supplemented with 100 μg/mL of ampicillin. Selected colonies were grown in Plasmid+ media, and the plasmids were extracted and purified using PureLink™ HiPure Plasmid Maxiprep Kit. Suspension HEK293F cells were grown in LV-MAX media and passaged to achieve a final cell density of ~5.5·10^6 viable cells/mL. Twelve hours before transfection, the cells were adjusted to a density of 3.5·10^6 cells/mL, cultured overnight, and diluted to a final concentration of 4.7·10^6 cells/mL. In a 125-mL flask, 25.5 mL of cell culture suspension was combined with 1.5 mL of LV-MAX supplement. In a 5-mL vial, 1.5 mL of OptiMEM I was mixed with 45 μg of LV-MAX Lentiviral Packaging Mix (a pre-defined mixture of plasmids pLP1, pLP2, and pLP/VSVG) and 30 μg of Vivid Colors™ pLenti6.3/V5-GW/ EmGFP Expression Control Vector plasmid. This mixture was slowly added to 1.5 mL of OptiMEM I and 180 μL of transfection reagent, and incubated at room temperature for 10 min. This mixture was slowly added to the viral production cells and placed in an incubator at 37°C and 8% CO_2 under gentle shaking at 125 rpm. After 6 h, 1.2 mL of LV-MAX enhancer was added to the cell suspension. The LV particles were harvested after 48 h by centrifugation at 1300g for 15 min, followed by filtration using 0.45 μm surfactant-free cellulose acetate (SFCA) filters (Thermo Fisher Scientific). All LV samples were immediately stored at −80°C until further use.

4.4 | Buffer stability studies

The clarified CCF containing LV particles was buffer exchanged using 7 kDa Zeba micro spin desalting columns (Thermo Fisher Scientific, Waltham, MA) against (i) 20 mM citrate buffer or 20 mM histidine buffer with 75 mM NaCl at the pH of either 6.0, 6.5, or 7.0; (ii) 20 mM PBS with 75 mM NaCl at the pH of either 6.2, 6.5, or 7.0; (iii) 20 mM citrate at pH 6.0 added with either 0.1, 0.25, or 0.5 M $MgCl_2$; or (iv) DMEM medium. Samples were incubated at room temperature for 30 min, followed by serial dilution in DMEM media supplemented with 8 μg/mL of polybrene. The LV titer in the samples was determined by transduction assay and the infectivity titers were expressed in comparison with LV samples in DMEM medium.

4.5 | Fluorescent labeling of LV particles, [E]VSV-G and [FL]VSV-G, and HEK293 HCPs

The NHS-ester dyes Alexafluor 594 (NHS-AF594, red) and NHS-Alexafluor 488 (NHS-AF488, green) were initially dissolved in DMSO at the concentration of 10 mg/mL. LV particles were purified by centrifugation following the procedure described by Jiang et al. (2015) and re-suspended in PBS at pH 7.4. The [E]VSV-G and [FL]VSV-G as well as the HEK293F CCF were buffer exchanged to PBS at pH 7.4 using Zeba spin desalting columns 7 kDa molecular weight cutoff (MWCO) (Thermo Fisher Scientific). Aliquots of 100 μL of LV particles (~10^11 vp/mL; ~10^9 TU/mL) or VSV-G protein (0.2 mg/mL) were mixed with 3 μL of dye NHS-AF488, and incubated at room temperature for 1 h under mild shaking and in the dark. The same procedure was used for labeling HEK293F HCPs (~0.3 mg/mL) with NHS-AF594. Unreacted dyes were removed by Zeba Dye removal column (Thermo Fisher Scientific) and the samples were stored at 4°C.

4.6 | Production and screening of the peptide library

A library of 8-mer linear peptides in the format $X_1X_2X_3X_4X_5X_6X_7X_8G$ was built following the split-couple-and-recombine method on Aminomethyl ChemMatrix resin via Fmoc/tBu chemistry using protected amino acids Fmoc-Ala-OH, Fmoc-Asn(Trt)-OH, Fmoc-Glu-(OtBu)-OH, Fmoc-Gly-OH, Fmoc-His(Trt)-OH, Fmoc-IleOH, Fmoc-Lys(Boc)-OH, Fmoc-Phe-OH, Fmoc-Ser(tBu)-OH, and Fmoc-Trp(Boc)-OH (Behrendt et al., 2016; Kilgore et al., 2023; Lam et al., 1991). Library synthesis was automated using a Syro I peptide synthesizer (Biotage, Uppsala, Sweden). Briefly, aliquots of resin in 5 mL reactor vials were combined with 3 equivalents (eq.) of protected amino acid at a concentration of 0.5 M in DMF, 3 eq. of HATU at 0.5 M in DMF, and 6 eq. of DIPEA at 0.5 M in NMP. Coupling was performed at 45°C for 20 min and followed by washing with DMF. After each reaction step, a Kaiser test was performed to

verify the completion of amino acid coupling. The Fmoc protection between two successive residues was removed using 20% v/v piperidine in DMF at room temperature. Upon completing chain elongation, the peptide library was deprotected via acidolysis using a cocktail of TFA:thionasole:EDT:anisole (90:5:3:2) for 2 h at room temperature. The deprotected library was then washed and stored in dry DMF.

Aliquots of 20 μL of peptide library beads were equilibrated with 20 mM phosphate buffer with 75 mM NaCl at pH 6.5 and combined with 200 μL of a screening mix comprising AF594-labeled HEK293T HCPs (~0.3 mg/mL) and either AF488-labeled LV (~10^{11} vp/mL; ~10^9 TU/mL) or AF488-labeled VSV-G protein (^{E}VSV-G or ^{FL}VSV-G, 0.2 mg/mL). After 30 min at room temperature, the beads were collected by centrifugation at 5000 g and resuspended in 200 mL of 20 mM phosphate buffer with 75 mM NaCl at pH 6.5. The library beads were screened using a microfluid device developed in prior work and installed on an Olympus IX81 fluorescent microscope (Center Valley, PA) (Barozzi et al., 2020; Chu et al., 2021, 2022; Day et al., 2019; Kilgore et al., 2023; Prodromou et al., 2021). Individual beads were imaged, and the values of green (AF488) and red (AF594) fluorescence emission were recorded; the bead was then washed for 5 min with 20 mM citrate buffer with 0.5 M MgCl$_2$, and imaged to record the new values of green and red fluorescence emission. All values of fluorescence emission, emission ratio, and emission reduction were determined in real time via image analysis using a custom MATLAB code (MathWorks) (Prodromou et al., 2023). The beads that exhibited (i) high green fluorescence emission and red-to-green emission ratio before washing and (ii) >75% reduction of green fluorescence emission after washing were isolated, while all other beads were discarded. The selected beads were finally analyzed via Edman degradation using a PPSQ-33A protein sequencer (Shimadzu) to sequence the candidate peptide ligands (note: based on the results of the Edman degradation, we estimate the purity of the peptide on the various resins to be at least above 83% and, in most cases, above 90%).

4.7 | In silico design of VSV-G-binding peptides and evaluation of VSV-G:peptide interactions

The crystal structure of the complex formed by the VSV-G and the LDL-R (PDB ID: 5OY9 and 5OYL) was analyzed to identify the paired residues and estimate their contributions to the binding energy. Nine designed sequences—namely, four disulfide-cyclic sequences (C-cyclo[GSRQFVADSDRD]C-GSG, C-cyclo[GSRSFVGDSDRD]C-GSG, C-cyclo[GSRAFVADADRD]C-GSG, C-cyclo[GSRAFVGDAD]C-GSG) and five linear sequences (SRQFVCGDSDRD-GSG, SRSFVCDSDRD-GSG, SRAFVGDADRD-GSG, AFVGDADRD-GSG, and SFVRIGLSD-GSG)—together with the sequences identified experimentally – namely FEKISNAE-GSG, FEKISAAE-GSG, FEKISTAE-GSG, GKEAAFAA-GSG, and SKSAAEHE-GSG – were constructed in Avogadro (Hanwell et al., 2012) and modeled in GROMACS using the force field GROMOS 54A7 (Schmid et al., 2011); briefly, each peptide sequence was (i)

placed in a simulation box with periodic boundary and containing 2000 TIP3P water molecules; (ii) equilibrated with 10,000 steps of steepest gradient descent; (iii) heated to 300K in an NVT ensemble for 250 ps using 1 fs time steps; and (iv) equilibrated to 1 atm via a 500-ps NPT simulation with 2 fs time steps. The production runs were then conducted in the NPT ensemble by applying the Nosé–Hoover thermostat (300K) and the Parrinello–Rahman barostat (1 atm), respectively (Ke et al., 2022); the motion equations were integrated using the leap-frog algorithm with steps of 2 fs; the LINCS algorithm was utilized to constrain the covalent bonds; the Lennard-Jones and short-range electrostatic interactions were calculated using cutoff values of 0.8 and 1.2 nm; the particle-mesh Ewald method was utilized for the long-range electrostatic interactions; (Schneible et al., 2019, 2020; Singhal et al., 2020) the lists of bonded and nonbonded interactions (cutoff of 1.2 nm) were updated every 2 and 6 fs. The structure of VSV-G was prepared using Protein Prep Wizard (PPW, Schrödinger) (Madhavi Sastry et al., 2013) by adding missing atoms and explicit hydrogens, removing salt ions and small ligands, and optimizing the hydrogen-bonding network. Two ionization states of VSV-G, one at pH 6.0 and one at 7.4—were obtained and subjected to structural minimization using PROPKA (Bas et al., 2008). The structures were then analyzed in SiteMap to identify putative peptide binding sites on VSV-G, namely the sites with high S-score (>0.8) and D-score (>0.9). The candidate peptide ligands were docked in silico against VSV-G at pH 6.0 and one at 7.4 using the docking software HADDOCK (High Ambiguity Driven Protein-Protein Docking) v.2.4 (Honorato et al., 2021; Van Zundert et al., 2016). The VSV-G residues present within the selected binding sites and the residues $X_1X_2[...]X_n$ on the peptides were denoted as "active"; all surrounding residues were marked as "passive". Clusters of VSV-G:peptide complexes with Cα RMSD < 7.5 Å were ranked using the dMM-PBSA score (Spiliotopoulos et al., 2016), and the top complexes were refined via 200-ns MD simulations to estimate the free energy of binding (ΔG_B).

4.8 | Amination and peptide conjugation of Poros™ 50 OH resin

A volume of 10 mL of Poros™ 50 OH resin was initially dried using a stream of nitrogen, washed in DMF, and resuspended in 50 mL of a solution of CDI at 100 mg/mL in DMF. Samples were kept under stirring and at room temperature. After 5 h, the resin was copiously washed with DMF and dried with a stream of nitrogen. The resin was then mixed with 100 mL of 5% v/v ethylenediamine in DMF, and incubated at 45°C under shaking at 100 rpm. After 12 h, the resin was washed with DMF, followed by DCM, dried with nitrogen, and stored at 4°C. The density of primary amine groups on modified Poros 50 resin beads was determined by Kaiser assay (Kaiser et al., 1970); briefly, 10 mg of resin was mixed with 1 mL of DMF, 0.1 mL of KCN in H$_2$O/pyridine, and 0.1 mL of ninhydrin, placed in boiling water for 5 min, and cooled down to room temperature; the supernatant was diluted 100-fold in DMF and the UV absorbance of the solution measured at 425 nm using a UV-1800 spectrophotometer

(Shimadzu); ethanolamine was used to build a calibration curve. The selected peptide sequences were synthesized on aminated Poros resin following the procedure outlined in Section 4.6 using an Alstra automated peptide synthesizer (Biotage).

4.9 | Purification of LV from HEK293 cell culture supernatant using peptide-Poros resins

The peptide-Poros resins were prepared as described in Section 4.8 and the control CaptureSelect™ Lenti VSVG and Poros™ 50 HE Heparin affinity resins were flow-packed in 1 mL Tricorn 5/50 columns (Cytiva) and installed on an AKTA Avant FPLC system (Cytiva). The resin packing quality was evaluated by measuring the peak symmetry of the conductivity signal generated by a pulse injection of aqueous 1 M NaCl (target value: 1–1.2). The resins were equilibrated with 10 CVs of equilibration buffer (Table 1). The clarified HEK293 CCF (LV titer ~0.5–2·10^8 TU/mL; HCP titer ~0.3 mg/mL; note: the ranges encompass the variability of LV activity across different production batches) was loaded on the resins at the RT of either 1 or 3.5 min. Following load, the resins were washed with 20 CVs of wash buffer, and the bound LVs were eluted with 9 CVs of elution buffer (Table 7). Following elution, the resins were regenerated using 10 CVs of 0.1 M glycine containing 2 M NaCl at pH 2.0.

4.10 | Measurements of dynamic binding capacity

GKEAAFAA-, FEKISNAE-, FEKISAAE-, and FEKISTAE-, SRAFV GDADRD-, and SFVRIGLSD-Poros resins prepared as described in Section 4.8 and the control CaptureSelect™ Lenti VSVG and Poros™ 50 HE Heparin affinity resins were flow-packed in 1 mL Tricorn 5/50 columns (Cytiva) and installed on an AKTA Avant FPLC system (Cytiva). Following equilibration with 10 CVs of 50 mM PIPES buffer with 100 mM NaCl buffer at pH 7.4, the resins were continuously loaded with clarified HEK293 CCF (LV titer ~0.5–2·10^8 TU/mL; HCP titer ~0.3 mg/mL) at the RT of either 1 or 2 min until the LV titer in the effluent reached 70%–80% of the corresponding feedstock titer. The effluent was apportioned in 3-mL fractions, which were analyzed

as described in Sections 4.12.2 and 4.12.3 to measure the titer of lentiviral genomes and transducing particles contained therein. The dynamic binding capacity at 10% of breakthrough ($DBC_{10\%}$) was calculated as described in prior work (Kish et al., 2017; Naik et al., 2019; Reese et al., 2020; Sripada et al., 2022; Xiao et al., 2022); the void volume of the system was measured via acetone pulse injection and utilized to adjust the value of $DBC_{10\%}$.

4.11 | Stability of the peptide-Poros resins

GKEAAFAA-, FEKISNAE-, FEKISAAE-, and FEKISTAE-, SRAFVG DADRD-, and SFVRIGLSD-Poros resins prepared as described in Section 4.8 and the control CaptureSelect™ Lenti VSVG and Poros™ 50 HE Heparin affinity resins were flow-packed in 1 mL Tricorn 5/50 columns (Cytiva), and installed on an AKTA Avant FPLC system (Cytiva). Following equilibration with 10 CVs of 50 mM PIPES buffer with 100 mM NaCl buffer at pH 7.4, the resins were loaded with 30 CVs of clarified HEK293 CCF (LV titer ~0.5–2·10^8 TU/mL; HCP titer ~0.3 mg/mL) at the RT of 1 min. After washing the resins with 20 CVs of binding buffer, the bound LVs were eluted with 4 CVs of 50 mM PIPES buffer with 650 mM NaCl buffer at pH 7.4 at the RT of 1 min. Following elution, the resins were regenerated with 10 CVs of 0.1 M glycine containing 2 M NaCl at pH 2.0 and subjected to CIP with 15 CVs of 0.5 M NaOH at the RT of 1 min followed by a static incubation for 30 min. Both regeneration and CIP steps were conducted at the RT of 1 min. An additional cycle of LV purification from the clarified HEK293 CCF with intermediate CIP was repeated. The chromatographic fractions were analyzed as described in Sections 4.12.1 and 4.12.4 to measure LV yield and purity.

4.12 | Analytical characterization of chromatographic fractions

4.12.1 | p24 ELISA and HEK293 HCP ELISA

The titer of p24 protein and HEK293 HCPs in the chromatographic samples was measured via ELISA using kits respectively by Abcam and Cygnus following the manufacturer's instructions.

TABLE 7 Composition of chromatographic buffers utilized for the purification of LVs using peptide-functionalized Poros resins.

Equilibration buffer	Wash buffer	Elution buffer
20 mM phosphate buffer	20 mM phosphate	20 mM citrate buffer
75 mM NaCl at pH 6.5	75 mM NaCl at pH 6.5 with or without 50 mM Arginine	0.5-1.0 M MgCl₂ at pH 6.0
50 mM Tris buffer	50 mM Tris buffer	50 mM Tris buffer
130 mM NaCl at pH 7.4	130 mM NaCl at pH 7.4	0.65 M NaCl at pH 7.4
50 mM HEPES buffer	50 mM HEPES buffer	50 mM HEPES buffer
100 mM NaCl at pH 7.4	100 mM NaCl at pH 7.4	0.65 M NaCl at pH 7.4
50 mM PIPES buffer	50 mM PIPES buffer	50 mM PIPES buffer
100 mM NaCl at pH 7.4	100 mM NaCl at pH 7.4	0.65 M NaCl at pH 7.4

TABLE 8 Primers and probe sequences for LV quantification by qPCR.

Primer	DNA sequence
Forward primer	CCCAGTTCCGCCCATTCTC
Reverse primer	GCCTCGGCCTCTGCATAAATAAA
Probe	ATGGCTGACTAATTTTT

4.12.2 | RT-qPCR

The chromatographic samples were initially treated with TurboD-NAse, followed by RNA isolation using a Purelink Viral RNA/DNA Kit (Thermo Fisher Scientific). The samples were then combined with TaqMan fast virus, custom TaqMan probe, and the primers listed in Table 8, and analyzed using a CFX Duet Real-Time qPCR System (Bio-Rad). Plasmid pLenti6.3/V5-GW/EmGFP was used as a standard.

4.12.3 | DNA quantification

The total amount of double-stranded DNA (dsDNA) was measured using Quant-iT™ PicoGreen™ dsDNA Assay Kits (Thermo Fisher Scientific) following the manufacturer's protocol.

4.12.4 | Fluorescence flow cytometry

HT1080 cells were seeded in a 96-well plate at the density of 7000 cells/well in high glucose DMEM media supplemented with Gluta-MAX™, pyruvate, and 10% v/v FBS. Plates were centrifuged at 900g for 5 min and placed in an incubator at 37°C and 5% CO_2. The chromatographic fractions containing LV particles were serially diluted (10×) in DMEM media supplemented with 8 µg/mL of polybrene (without FBS or antibiotics). After 4 h, the spent cell culture medium in the 96-well plates was replaced with 0.1 mL of diluted samples and incubated for 12 h. The samples were then replaced with fresh DMEM media supplemented with 10% v/v FBS. After 60 h, the cells were detached from the plate via incubation with 150 µL of a mixture composed of TrypLE™ Express Enzyme:DPBS (75:25 v:v) for 15 min at 37°C. The fraction of cells expressing GFP (GFP$^+$) was quantified using a CytoFlex flow cytometer (Beckman Coulter) and the number of transduction units per mL (TU/mL) was calculated using Equation (1):

$$\text{Transducing units}\left(\frac{\text{TU}}{\text{mL}}\right) = \frac{N_{\text{HT1080}} \times \%\text{GFP}^+}{V \times \text{DF}} \quad (1)$$

Wherein N_{HT1080} is the number of cells incubated with the diluted AAV sample, V is the volume of the diluted AAV sample, and DF is the dilution factor. Each sample was analyzed in triplicate.

AUTHOR CONTRIBUTIONS

Eduardo Barbieri, Gina N. Mollica, Brandyn D. Moore, Sobhana A. Sripada, Ryan E. Kilgore, Shriarjun Shastry, Casee M. Loudermilk, Zachary H. Whitacre, and Katie M. Kilgour conducted the experimental work. Elena Wuestenhagen, Annika Aldinger, Heiner Graalfs, Oliver Rammo, Michael M. Schulte, Michael A. Daniele, Thomas F. Johnson, and Stefano Menegatti conceived the work. Eduardo Barbieri and Stefano Menegatti wrote the manuscript.

CONFLICT OF INTEREST STATEMENT

The authors declare no conflict of interest.

DATA AVAILABILITY STATEMENT

The data that support the findings of this study are available from the corresponding author upon reasonable request.

ORCID

Sobhana A. Sripada http://orcid.org/0000-0003-2011-8527
Thomas F. Johnson http://orcid.org/0000-0001-6494-2206
Stefano Menegatti http://orcid.org/0000-0001-5633-434X

REFERENCES

Adams, B., Bak, H., & Tustian, A. D. (2020). Moving from the bench towards a large scale, industrial platform process for adeno-associated viral vector purification. *Biotechnology and Bioengineering*, 117, 3199–3211.

Akkina, R. K., Walton, R. M., Chen, M. L., Li, Q. X., Planelles, V., & Chen, I. S. (1996). High-efficiency gene transfer into CD34 cells with a human immunodeficiency virus type 1-based retroviral vector pseudotyped with vesicular stomatitis virus envelope glycoprotein G. *Journal of Virology*, 70, 2581–2585.

Alele, N., & Ulbricht, M. (2016). Membrane-based purification of proteins from nanoparticle dispersions: Influences of membrane type and ultrafiltration conditions. *Separation and Purification Technology*, 158, 171–182.

Bacon, K., Bowen, J., Reese, H., Rao, B. M., & Menegatti, S. (2020). Use of target-displaying magnetized yeast in screening mRNA-Display peptide libraries to identify ligands. *ACS Combinatorial Science*, 22, 738–744.

Bandeira, V., Peixoto, C., Rodrigues, A. F., Cruz, P. E., Alves, P. M., Coroadinha, A. S., & Carrondo, M. J. T. (2012). Downstream processing of lentiviral vectors: Releasing bottlenecks. *Human Gene Therapy Methods*, 23, 255–263.

Barozzi, A., Lavoie, R. A., Day, K. N., Prodromou, R., & Menegatti, S. (2020). Affibody-binding ligands. *International Journal of Molecular Sciences*, 21, 3769.

Bas, D. C., Rogers, D. M., & Jensen, J. H. (2008). Very fast prediction and rationalization of pKa values for protein-ligand complexes. *Proteins: Structure, Function, and Bioinformatics*, 73, 765–783.

Behrendt, R., White, P., & Offer, J. (2016). Advances in Fmoc solid-phase peptide synthesis. *Journal of Peptide Science*, 22, 4–27.

Bellmaine, S., Schnellbaecher, A., & Zimmer, A. (2020). Reactivity and degradation products of tryptophan in solution and proteins. *Free Radical Biology and Medicine*, 160, 696–718.

Birger Anspach, F., Spille, H., & Rinas, U. (1995). Purification of recombinant human basic fibroblast growth factor: Stability of selective sorbents under cleaning in place conditions. *Journal of Chromatography A*, 711, 129–139.

Bray, B. L. (2003). Large-scale manufacture of peptide therapeutics by chemical synthesis. *Nature Reviews Drug Discovery*, 2, 587–593.

Burns, J. C., Friedmann, T., Driever, W., Burrascano, M., & Yee, J. K. (1993). Vesicular stomatitis virus G glycoprotein pseudotyped retroviral vectors: Concentration to very high titer and efficient gene transfer into mammalian and nonmammalian cells. *Proceedings of the National Academy of Sciences of the United States of America*, 90, 8033–8037.

Carvalho, S. B., Silva, R. J. S., Moreira, A. S., Cunha, B., Clemente, J. J., Alves, P. M., Carrondo, M. J. T., Xenopoulos, A., & Peixoto, C. (2019). Efficient filtration strategies for the clarification of influenza virus-like particles derived from insect cells. *Separation and Purification Technology*, 218, 81–88.

Cheeks, M. C., Kamal, N., Sorrell, A., Darling, D., Farzaneh, F., & Slater, N. K. H. (2009). Immobilized metal affinity chromatography of histidine-tagged lentiviral vectors using monolithic adsorbents. *Journal of Chromatography A*, 1216, 2705–2711.

Chin, K., G-x, G. L., & P-y Ting, J. (1997). Importance of acidic, proline serine threonine-rich, and GTP-binding regions in the major histocompatibility complex class II transactivator: Generation of transdominant-negative mutants. *Immunology*, 94, 2501–2506.

Chu, W., Prodromou, R., Moore, B., Elhanafi, D., Kilgore, R., Shastry, S., & Menegatti, S. (2022). Development of peptide ligands for the purification of α−1 antitrypsin from cell culture fluids. *Journal of Chromatography A*, 1679, 463363.

Chu, W., Shastry, S., Barbieri, E., Prodromou, R., Greback-Clarke, P., Smith, W., Moore, B., Kilgore, R., Cummings, C., Pancorbo, J., Gilleskie, G., Daniele, M. A., & Menegatti, S. (2023). Peptide ligands for the affinity purification of adeno-associated viruses from HEK 293 cell lysates. *Biotechnology and Bioengineering*, 120, 2283–2300.

Chu, W., Prodromou, R., Day, K. N., Schneible, J. D., Bacon, K. B., Bowen, J. D., Kilgore, R. E., Catella, C. M., Moore, B. D., Mabe, M. D., Alashoor, K., Xu, Y., Xiao, Y., & Menegatti, S. (2021). Peptides and pseudopeptide ligands: A powerful toolbox for the affinity purification of current and next-generation biotherapeutics. *Journal of Chromatography A*, 1635, 461632.

Ci, Y., Yang, Y., Xu, C., & Shi, L. (2018). Vesicular stomatitis virus G protein transmembrane region is crucial for the hemi-fusion to full fusion transition. *Scientific Reports*, 8, 10669.

Cleverley, D. Z., & Lenard, J. (1998). The transmembrane domain in viral fusion: Essential role for a conserved glycine residue in vesicular stomatitis virus G protein. *Proceedings of the National Academy of Sciences of the United States of America*, 95, 3425–3430.

Coil, D. A., & Miller, A. D. (2004). Phosphatidylserine is not the cell surface receptor for vesicular stomatitis virus. *Journal of Virology*, 78, 10920–10926.

Coroadinha, A. S., Silva, A. C., Pires, E., Coelho, A., Alves, P. M., & Carrondo, M. J. T. (2006). Effect of osmotic pressure on the production of retroviral vectors: Enhancement in vector stability. *Biotechnology and Bioengineering*, 94, 322–329.

Crespo-Barreda, A., Encabo-Berzosa, M. M., González-Pastor, P., Iglesias, M., Serrano, J. L., & Martin-Duque, P. (2016). Viral and nonviral vectors for in vivo and ex vivo gene therapies, *Translating regenerative medicine to the clinic* (pp. 155–177).

Cribbs, A. P., Kennedy, A., Gregory, B., & Brennan, F. M. (2013). Simplified production and concentration of lentiviral vectors to achieve high transduction in primary human T cells. *BMC Biotechnology*, 13, 98.

Croyle, M. A., Callahan, S. M., Auricchio, A., Schumer, G., Linse, K. D., Wilson, J. M., Brunner, L. J., & Kobinger, G. P. (2004). PEGylation of a vesicular stomatitis virus G pseudotyped lentivirus vector prevents inactivation in serum. *Journal of Virology*, 78, 912–921.

Dautzenberg, I. J. C., Rabelink, M. J. W. E., & Hoeben, R. C. (2021). The stability of envelope-pseudotyped lentiviral vectors. *Gene Therapy*, 28, 89–104.

Day, K., Prodromou, R., Saberi Bosari, S., Lavoie, A., Omary, M., Market, C., San Miguel, A., & Menegatti, S. (2019). Discovery and evaluation of peptide ligands for selective adsorption and release of Cas9 nuclease on solid substrates. *Bioconjugate Chemistry*, 30, 3057–3068.

Deb, A., Nebelitsky, E., & Slepushkin, V. (2017). WO2017087861A1, pp. 1–84.

Donas, R. W., Ruusala, A., Machamer, C., Helenius, J., Helenius, A., & Rose, J. K. (1988). Differential effects of mutations in three domains on folding, quaternary structure, and intracellular transport of vesicular stomatitis virus G protein. *The Journal of Cell Biology*, 107(1), 89–99.

Escors, D., & Breckpot, K. (2010). Lentiviral vectors in gene therapy: Their current status and future potential. *Archivum Immunologiae et Therapiae Experimentalis*, 58, 107–119.

Ferlin, A., Raux, H., Baquero, E., Lepault, J., & Gaudin, Y. (2014). Characterization of pH-sensitive molecular switches that trigger the structural transition of vesicular stomatitis virus glycoprotein from the postfusion state toward the prefusion state. *Journal of Virology*, 88, 13396–13409.

Finkelshtein, D., Werman, A., Novick, D., & Rubinstein, M. (2013). LDL receptor and its family members serve as the cellular receptors for vesicular stomatitis virus. *Proceedings of the National Academy of Sciences of the United States of America*, 110, 7306–7311.

Florea, M., Nicolaou, F., Pacouret, S., Zinn, E. M., Sanmiguel, J., Andres-Mateos, E., Unzu, C., Wagers, A. J., & Vandenberghe, L. H. (2023). High-efficiency purification of divergent AAV serotypes using AAVX affinity chromatography. *Molecular Therapy - Methods & Clinical Development*, 28, 146–159.

Food and Drug Administration. (2013). *Guidance for industry heparin for drug and medical device use: Monitoring crude heparin for quality*.

Fortuna, A. R., van Teeffelen, S., Ley, A., Fischer, L. M., Taft, F., Genzel, Y., Villain, L., Wolff, M. W., & Reichl, U. (2019). Use of sulfated cellulose membrane adsorbers for chromatographic purification of cell cultured-derived influenza A and B viruses. *Separation and Purification Technology*, 226, 350–358.

Frejd, F. Y., & Kim, K.-T. (2017). Affibody molecules as engineered protein drugs. *Experimental & Molecular Medicine*, 49, e306.

Gao, Z. Y., Zhang, Q. L., Shi, C., Gou, J. X., Gao, D., Wang, H. B., Yao, S. J., & Lin, D. Q. (2020). Antibody capture with twin-column continuous chromatography: Effects of residence time, protein concentration and resin. *Separation and Purification Technology*, 253, 117554.

Ghosh, R., Koley, S., Gopal, S., Rodrigues, A. L., Dordick, J. S., & Cramer, S. M. (2022). Evaluation of lentiviral vector stability and development of ion exchange purification processes. *Biotechnology Progress*, 38, e3286.

Gibco. (2021). *LV-MAX™ Lentiviral production system—User guide*. https://assets.thermofisher.com/TFS-Assets/LSG/manuals/MAN0017000_LV_MAX_ViralProductionSystem_UG.pdf

Gülich, S., Linhult, M., Nygren, P. Å., Uhlén, M., & Hober, S. (2000). Stability towards alkaline conditions can be engineered into a protein ligand. *Journal of Biotechnology*, 80, 169–178.

Han, X. (2012). Optogenetics in the nonhuman primate. *Progress in Brain Research*, 196, 215–233.

Hanawa, H., Kelly, P. F., Nathwani, A. C., Persons, D. A., Vandergriff, J. A., Hargrove, P., Vanin, E. F., & Nienhuis, A. W. (2002). Comparison of various envelope proteins for their ability to pseudotype lentiviral vectors and transduce primitive hematopoietic cells from human blood. *Molecular Therapy*, 5, 242–251.

Hanwell, M. D., Curtis, D. E., Lonie, D. C., Vandermeersch, T., Zurek, E., & Hutchison, G. R. (2012). Avogadro: An advanced semantic chemical editor, visualization, and analysis platform. *Journal of Cheminformatics*, 4, 17.

Hayashi-Takanaka, Y., Stasevich, T. J., Kurumizaka, H., Nozaki, N., & Kimura, H. (2014). Evaluation of chemical fluorescent dyes as a protein conjugation partner for live cell imaging. *PLoS One*, 9, e106271.

Higashikawa, F., & Chang, L. J. (2001). Kinetic analyses of stability of simple and complex retroviral vectors. *Virology*, 280, 124–131.

Honorato, R. V., Koukos, P. I., Jiménez-García, B., Tsaregorodtsev, A., Verlato, M., Giachetti, A., Rosato, A., & Bonvin, A. M. J. J. (2021). Structural biology in the clouds: The WeNMR-EOSC ecosystem. *Frontiers in Molecular Biosciences*, 8, 729513.

Horenstein, A. L., Crivellin, F., Funaro, A., Said, M., & Malavasi, F. (2003). Design and scaleup of downstream processing of monoclonal antibodies for cancer therapy: From research to clinical proof of principle. *Journal of Immunological Methods*, 275, 99–112.

Jiang, W., Hua, R., Wei, M., Li, C., Qiu, Z., Yang, X., & Zhang, C. (2015). An optimized method for high-titer lentivirus preparations without ultracentrifugation. *Scientific Reports*, 5, 13875.

Kaiser, E., Colescott, R. L., Bossinger, C. D., & Cook, P. I. (1970). Color test for detection of free terminal amino groups in the solid-phase synthesis of peptides. *Analytical Biochemistry*, 34, 595–598.

Kato, K., Nakayoshi, T., Kurimoto, E., & Oda, A. (2020). Mechanisms of deamidation of asparagine residues and effects of main-chain conformation on activation energy. *International Journal of Molecular Sciences*, 21, 7035.

Kawka, K., Wilton, A. N., Madadkar, P., Medina, M. F. C., Lichty, B. D., Ghosh, R., & Latulippe, D. R. (2021). Integrated development of enzymatic DNA digestion and membrane chromatography processes for the purification of therapeutic adenoviruses. *Separation and Purification Technology*, 254, 117503.

Ke, Q., Gong, X., Liao, S., Duan, C., & Li, L. (2022). Effects of thermostats/barostats on physical properties of liquids by molecular dynamics simulations. *Journal of Molecular Liquids*, 365, 120116.

Kilgore, R., Chu, W., Bhandari, D., Fischler, D., Carbonell, R. G., Crapanzano, M., & Menegatti, S. (2023). Development of peptide affinity ligands for the purification of polyclonal and monoclonal Fabs from recombinant fluids. *Journal of Chromatography A*, 1687, 463701.

Kish, W. S., Hiroyuki, S., Amith, D. N., Matthew, K. R., Benjamin, G. B., Robert, K. B., Stefano, M., & Ruben, G. C. (2017). Design, selection, and development of cyclic peptide ligands for human erythropoietin. *Journal of Chromatography A*, 1500, 105–120.

Kozorog, M., Caserman, S., Grom, M., Vicente, F. A., Pohar, A., & Likozar, B. (2023). Model-based process optimization for mAb chromatography. *Separation and Purification Technology*, 305, 122528.

Kumru, O. S., Wang, Y., Gombotz, C. W. R., Kelley-Clarke, B., Cieplak, W., Kim, T., Joshi, S. B., & Volkin, D. B. (2018). Physical characterization and stabilization of a lentiviral vector against adsorption and freeze-thaw. *Journal of Pharmaceutical Sciences*, 107, 2764–2774.

Kutner, R. H., Zhang, X.-Y., & Reiser, J. (2009). Production, concentration and titration of pseudotyped HIV-1-based lentiviral vectors. *Nature Protocols*, 4, 495–505.

Łącki, K. M., & Riske, F. J. (2020). Affinity chromatography: an enabling technology for large-scale bioprocessing. *Biotechnology Journal*, 15, e1800397.

Lam, K. S., Salmon, S. E., Hersh, E. M., Hruby, V. J., Kazmierski, W. M., & Knapp, R. J. (1991). A new type of synthetic peptide library for identifying ligand-binding activity. *Nature*, 354, 82–84.

de las Mercedes Segura, M., Kamen, A., & Garnier, A. (2008). Purification of retrovirus particles using heparin affinity chromatography. In J. M. le Doux (Ed.), *Gene therapy protocols: Design and characterization of gene transfer vectors* (pp. 1–11). Humana Press.

Lavoie, R., di Fazio, A., Blackburn, R., Goshe, M., Carbonell, R., & Menegatti, S. (2019). Targeted capture of Chinese hamster ovary host cell proteins: Peptide ligand discovery. *International Journal of Molecular Sciences*, 20, 1729.

Lavoie, R. A., di Fazio, A., Williams, T. I., Carbonell, R., & Menegatti, S. (2020). Targeted capture of Chinese hamster ovary host cell proteins: Peptide ligand binding by proteomic analysis. *Biotechnology and Bioengineering*, 117, 438–452.

Lavoie, R. A., Chu, W., Lavoie, J. H., Hetzler, Z., Williams, T. I., Carbonell, R., & Menegatti, S. (2021). Removal of host cell proteins from cell culture fluids by weak partitioning chromatography using peptide-based adsorbents. *Separation and Purification Technology*, 257, 117890.

Leung, S., McLeod, A. T., Sheikholeslami, Z., Shoaebargh, S., Ho, T., Ramanuj, R., Beaudette, P., Bakhtyar, N., & Ghorbani, A. (2020). Building a robust and scalable lentiviral vector purification platform. *Cytotherapy*, 22, S184–S185.

van Lieshout, L. P., Stegelmeier, A. A., Rindler, T. N., Lawder, J. J., Sorensen, D. L., Frost, K. L., Booth, S. A., Bridges, J. P., & Wootton, S. K. (2023). Engineered AAV8 capsid acquires heparin and AVB sepharose binding capacity but has altered in vivo transduction efficiency. *Gene Therapy*, 30, 236–244.

Linhult, M., Gülich, S., Gräslund, T., Simon, A., Karlsson, M., Sjöberg, A., Nord, K., & Hober, S. (2004). Improving the tolerance of a protein A analogue to repeated alkaline exposures using a bypass mutagenesis approach. *Proteins: Structure, Function, and Bioinformatics*, 55, 407–416.

Madhavi Sastry, G., Adzhigirey, M., Day, T., Annabhimoju, R., & Sherman, W. (2013). Protein and ligand preparation: Parameters, protocols, and influence on virtual screening enrichments. *Journal of Computer-Aided Molecular Design*, 27, 221–234.

Matos, M. J. B., Trovão, F., Gonçalves, J., Rothbauer, U., Freire, M. G., Barbosa, A. M. J. B., Pina, A. S., & Roque, A. C. A. (2021). A purification platform for antibodies and derived fragments using a de novo designed affinity adsorbent. *Separation and Purification Technology*, 265, 118476.

Mazzer, A. R., Perraud, X., Halley, J., O'Hara, J., & Bracewell, D. G. (2015). Protein A chromatography increases monoclonal antibody aggregation rate during subsequent low pH virus inactivation hold. *Journal of Chromatography A*, 1415, 83–90.

McNally, D. J., Darling, D., Farzaneh, F., Levison, P. R., & Slater, N. K. H. (2014). Optimised concentration and purification of retroviruses using membrane chromatography. *Journal of Chromatography A*, 1340, 24–32.

Mekkaoui, L., Parekh, F., Kotsopoulou, E., Darling, D., Dickson, G., Cheung, G. W., Chan, L., MacLellan-Gibson, K., Mattiuzzo, G., Farzaneh, F., Takeuchi, Y., & Pule, M. (2018). Lentiviral vector purification using genetically encoded biotin mimic in packaging cell. *Molecular Therapy – Methods & Clinical Development*, 11, 155–165.

Minh, A., & Kamen, A. A. (2021). Critical assessment of purification and analytical technologies for enveloped viral vector and vaccine processing and their current limitations in resolving co-expressed extracellular vesicles. *Vaccines*, 9, 823.

Moleirinho, M. G., Feast, S., Moreira, A. S., Silva, R. J. S., Alves, P. M., Carrondo, M. J. T., Huber, T., Fee, C., & Peixoto, C. (2021). 3D-printed ordered bed structures for chromatographic purification of enveloped and non-enveloped viral particles. *Separation and Purification Technology*, 254, 117681.

Moleirinho, M. G., Fernandes, R. P., Carvalho, S. B., Bezemer, S., Detmers, F., Hermans, P., Silva, R. J. S., Alves, P. M., Carrondo, M. J. T., & Peixoto, C. (2020). Baculovirus affinity removal in viral-based bioprocesses. *Separation and Purification Technology*, 241, 116693.

Moreira, A. S., Cavaco, D. G., Faria, T. Q., Alves, P. M., Carrondo, M. J. T., & Peixoto, C. (2021). Advances in lentivirus purification. *Biotechnology Journal*, 16, e2000019.

Moreira, A. S., Bezemer, S., Faria, T. Q., Detmers, F., Hermans, P., Sierkstra, L., Coroadinha, A. S., & Peixoto, C. (2023). Implementation of novel affinity ligand for lentiviral vector purification. *International Journal of Molecular Sciences*, 24, 3354.

Moreira, A. S., Faria, T. Q., Oliveira, J. G., Kavara, A., Schofield, M., Sanderson, T., Collins, M., Gantier, R., Alves, P. M., Carrondo, M. J. T., & Peixoto, C. (2021). Enhancing the purification of Lentiviral vectors for clinical applications. *Separation and Purification Technology*, 274, 118598.

Naik, A. D., Islam, T., Terasaka, T., Ohara, Y., Hashimoto, Y., Menegatti, S., & Carbonell, R. (2019). Silica resins and peptide ligands to develop disposable affinity adsorbents for antibody purification. *Biochemical Engineering Journal*, 145, 53–61.

Naldini, L., Blömer, U., Gallay, P., Ory, D., Mulligan, R., Gage, F. H., Verma, I. M., & Trono, D. (1996). In vivo gene delivery and stable transduction of nondividing cells by a lentiviral vector. *Science*, 272, 263–267.

Nass, S. A., Mattingly, M. A., Woodcock, D. A., Burnham, B. L., Ardinger, J. A., Osmond, S. E., Frederick, A. M., Scaria, A., Cheng, S. H., & O'Riordan, C. R. (2018). Universal method for the purification of recombinant AAV vectors of differing serotypes. *Molecular Therapy – Methods & Clinical Development*, 9, 33–46.

Nikolic, J., Belot, L., Raux, H., Legrand, P., Gaudin, Y., & A. Albertini, A. (2018). Structural basis for the recognition of LDL-receptor family members by VSV glycoprotein. *Nature Communications*, 9, 1029.

Pagliarulo, N. W. (2022). With $2.8M gene therapy, Bluebird sets new bar for US drug pricing. *BioPharma Dive*.

Perry, C., & Rayat, A. C. M. E. (2021). Lentiviral vector bioprocessing. *Viruses*, 13(2), 268.

Priori, S. G., Denegri, M., Bongianino, R., & Napolitano, C. (2018). Gene therapy to treat cardiac arrhythmias, *Cardiac electrophysiology: From cell to bedside* (7th ed., pp. 531–540).

Prodromou, R., Day, K. N., Saberi-Bosari, S., Schneible, J. D., Mabe, M. D., San Miguel, A., Daniele, M. A., Pozdin, V., & Menegatti, S. (2021). Engineering next generation cyclized peptide ligands for light-controlled capture and release of therapeutic proteins. *Advanced Functional Materials*, 31, 2101410.

Prodromou, R., Moore, B. D., Chu, W., Deal, H., San Miguel, A., Brown, A. C., Daniele, M. A. A., Pozdin, V. A., & Menegatti, S. (2023). Molecular engineering of cyclic azobenzene-peptide hybrid ligands for the purification of human blood factor VIII via photo-affinity chromatography. *Advanced Functional Materials*, 33, 2213881.

Reese, H. R., Xiao, X., Shanahan, C. C., Chu, W., Van Den Driessche, G. A., Fourches, D., Carbonell, R. G., Hall, C. K., & Menegatti, S. (2020). Novel peptide ligands for antibody purification provide superior clearance of host cell protein impurities. *Journal of Chromatography A*, 1625, 461237.

Reiser, J., Harmison, G., Kluepfel-Stahl, S., Brady, R. O., Karlsson, S., & Schubert, M. (1996). Transduction of nondividing cells using pseudotyped defective high-titer HIV type 1 particles. *Proceedings of the National Academy of Sciences of the United States of America*, 93, 15266–15271.

Robbins, P. D., Storkus, W. J., & Gambotto, A. (2003). Cytokine gene transfer, *The cytokine handbook* (pp. 1335–1348).

Rodrigues, T., Alves, A., Lopes, A., Carrondo, M. J. T., Alves, P. M., & Cruz, P. E. (2008). Removal of envelope protein-free retroviral vectors by anion-exchange chromatography to improve product quality. *Journal of Separation Science*, 31, 3509–3518.

Ruscic, J., Perry, C., Mukhopadhyay, T., Takeuchi, Y., & Bracewell, D. G. (2019). Lentiviral vector purification using nanofiber ion-exchange chromatography. *Molecular Therapy - Methods & Clinical Development*, 15, 52–62.

Salvi, G., De Los Rios, P., & Vendruscolo, M. (2005). Effective interactions between chaotropic agents and proteins. *Proteins: Structure, Function, and Bioinformatics*, 61, 492–499.

Schmid, N., Eichenberger, A. P., Choutko, A., Riniker, S., Winger, M., Mark, A. E., & van Gunsteren, W. F. (2011). Definition and testing of the GROMOS force-field versions 54A7 and 54B7. *European Biophysics Journal*, 40, 843–856.

Schneible, J. D., Singhal, A., Lilova, R. L., Hall, C. K., Grafmüller, A., & Menegatti, S. (2019). Tailoring the chemical modification of chitosan hydrogels to fine-tune the release of a synergistic combination of chemotherapeutics. *Biomacromolecules*, 20, 3126–3141.

Schneible, J. D., Shi, K., Young, A. T., Ramesh, S., He, N., Dowdey, C. E., Dubnansky, J. M., Lilova, R. L., Gao, W., Santiso, E., Daniele, M., & Menegatti, S. (2020). Modified gaphene oxide (GO) particles in peptide hydrogels: a hybrid system enabling scheduled delivery of synergistic combinations of chemotherapeutics. *Journal of Materials Chemistry B*, 8, 3852–3868.

Segura, M. M., Kamen, A. A., & Garnier, A. (2011). Overview of current scalable methods for purification of viral vectors. *in Methods in Molecular Biology*, 737, 89–116.

Segura, M. M., Garnier, A., Durocher, Y., Coelho, H., & Kamen, A. (2007). Production of lentiviral vectors by large-scale transient transfection of suspension cultures and affinity chromatography purification. *Biotechnology and Bioengineering*, 98, 789–799.

Singhal, A., Schneible, J. D., Lilova, R. L., Hall, C. K., Menegatti, S., & Grafmüller, A. (2020). A multiscale coarse-grained model to predict the molecular architecture and drug transport properties of modified chitosan hydrogels. *Soft Matter*, 16, 10591–10610.

Spiliotopoulos, D., Kastritis, P. L., Melquiond, A. S. J., Bonvin, A. M. J. J., Musco, G., Rocchia, W., & Spitaleri, A. (2016). dMM-PBSA: A new HADDOCK scoring function for protein-peptide docking. *Frontiers in Molecular Biosciences*, 3, 46.

Sripada, S. A., Elhanafi, D., Collins, L. B., Williams, T. I., Linova, M. Y., Woodley, J. M., Boi, C., & Menegatti, S. (2023). Pseudo-affinity capture of *K. phaffii* host cell proteins in flow-through mode: purification of protein therapeutics and proteomic study. *Separation and Purification Technology*, 326, 124777.

Sripada, S. A., Chu, W., Williams, T. I., Teten, M. A., Mosley, B. J., Carbonell, R. G., Lenhoff, A. M., Cramer, S. M., Bill, J., Yigzaw, Y., Roush, D. J., & Menegatti, S. (2022). Towards continuous mAb purification: Clearance of host cell proteins from CHO cell culture harvests via "flow-through affinity chromatography" using peptide-based adsorbents. *Biotechnology and Bioengineering*, 119, 1873–1889.

Sun, L., Li, H., Qu, L., Zhu, R., Fan, X., Xue, Y., Xie, Z., & Fan, H. (2014). Immobilized lentivirus vector on chondroitin sulfate-hyaluronate acid-silk fibroin hybrid scaffold for tissue-engineered ligament-bone junction. *BioMed Research International*, 2014, 816979.

Surade, S., & Blundell, T. L. (2012). Structural biology and drug discovery of difficult targets: The limits of ligandability. *Chemistry & Biology*, 19, 42–50.

ThermoFisher. (2023). *CaptureSelect™ Lenti VSVG Affinity Matrix*. https://www.thermofisher.com/order/catalog/product/2943932050

U.S. Food and Drug Administration. (2021). *ABECMA BL 125736/0 Approval Letter* (Preprint at 2021).

U.S. Food and Drug Administration. (2022a). *CARVYKTI BL 125746/0 Approval Letter* (Preprint at 2022a).

U.S. Food and Drug Administration. (2022b). *BREYANZI BL 125714/90 Approval letter* (Preprint at 2022b).

U.S. Food and Drug Administration. (2022c). *SKYSONA BL 125755/0 Approval Letter* (Preprint at 2022c).

U.S. Food and Drug Administration. (2022d). *ZYNTEGLO BL 125717/0 Approval Letter* (Preprint at 2022d).

Van der Meer, J.-Y., Kellenbach, E., & Van den Bos, L. (2017). From farm to pharma: An overview of industrial heparin manufacturing methods. *Molecules*, *22*, 1025.

Van Zundert, G. C. P., Rodrigues, J. P. G. L. M., Trellet, M., Schmitz, C., Kastritis, P. L., Karaca, E., Melquiond, A. S. J., van Dijk, M., de Vries, S. J., & Bonvin, A. M. J. J. (2016). The HADDOCK2.2 web server: User-friendly integrative modeling of biomolecular complexes. *Journal of Molecular Biology*, *428*, 720–725.

Vazquez-Lombardi, R., Phan, T. G., Zimmermann, C., Lowe, D., Jermutus, L., & Christ, D. (2015). Challenges and opportunities for non-antibody scaffold drugs. *Drug Discovery Today*, *20*, 1271–1283.

Vigna, E., & Naldini, L. (2000). Lentiviral vectors: Excellent tools for experimental gene transfer and promising candidates for gene therapy. *The Journal of Gene Medicine*, *2*, 308–316.

Volland, A., Lohmüller, M., Heilmann, E., Kimpel, J., Herzog, S., & von Laer, D. (2021). Heparan sulfate proteoglycans serve as alternative receptors for low affinity LCMV variants. *PLOS Pathogens*, *17*, e1009996.

Wang, R., Lu, Y., & Wang, S. (2003). Comparative evaluation of 11 scoring functions for molecular docking. *Journal of Medicinal Chemistry*, *46*, 2287–2303.

Xia, H.-F., Liang, Z.-D., Wang, S.-L., Wu, P.-Q., & Jin, X.-H. (2014). Molecular modification of protein A to improve the elution ph and alkali resistance in affinity chromatography. *Applied Biochemistry and Biotechnology*, *172*, 4002–4012.

Xiao, X., Kilgore, R., Sarma, S., Chu, W., Menegatti, S., & Hall, C. K. (2022). De novo discovery of peptide-based affinity ligands for the fab fragment of human immunoglobulin G. *Journal of Chromatography A*, *1669*, 462941.

Yaniz-Galende, E., & Hajjar, R. J. (2014). Stem cell and gene therapy for cardiac regeneration. *Cardiac Regeneration and Repair*, *1*, 347–379.

Ye, K., Dhiman, H. K., Suhan, J., & Schultz, J. S. (2003). Effect of pH on infectivity and morphology of ecotropic moloney murine leukemia virus. *Biotechnology Progress*, *19*, 538–543.

Ye, K., Jin, S., Ataai, M. M., Schultz, J. S., & Ibeh, J. (2004). Tagging retrovirus vectors with a metal binding peptide and one-step purification by immobilized metal affinity chromatography. *Journal of Virology*, *78*, 9820–9827.

Zhang, C., Fredericks, D., Campi, E. M., Florio, P., Jespersgaard, C., Schiødt, C. B., & Hearn, M. T. W. (2015). Purification of monoclonal antibodies by chemical affinity mixed mode chromatography. *Separation and Purification Technology*, *142*, 332–339.

Zhang, J., Siva, S., Caple, R., Ghose, S., & Gronke, R. (2017). Maximizing the functional lifetime of Protein A resins. *Biotechnology Progress*, *33*, 708–715.

Zhou, H.-X., & Pang, X. (2018). Electrostatic interactions in protein structure, folding, binding, and condensation. *Chemical Reviews*, *118*, 1691–1741.

SUPPORTING INFORMATION

Additional supporting information can be found online in the Supporting Information section at the end of this article.